Curating Glioma Tumors for Classification Methods in Machine Learning
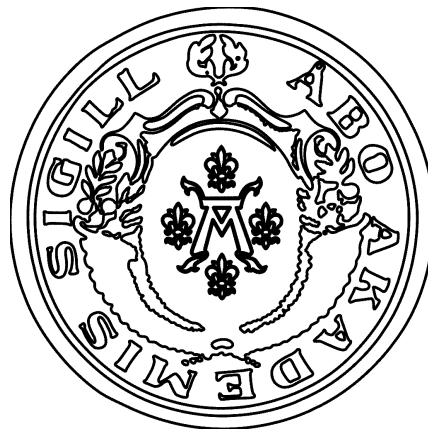
Author:

JOEL SJÖBERG, 38686

Supervisor:

ADJ PROF LUIGIA PETRE

Masters thesis in computer science

The Faculty Of Science And Engineering

Åbo Akademi University

Finland

2021

Contents

Foreword

This thesis would not have been possible without the supervision and support of Luigia Petre, whose patient attitude and rigorous feedback has provided me great inspiration in writing and expanding each chapter. I would also like to thank Ion Petre, who generously allowed me to take part in the project this thesis covers, and for his encouragement and support. I thank my parents and extended family, who all have suffered through lengthy discussions and explanations about this project and other jargon related to my area of study. And my fellow peers, whom I have had the exceptional and delightful privilege of meeting. Our long discussions about our studies have fueled my enthusiasm since my first year as a student, and will continue to do so for years to come. I would especially like to thank Patric Gustafsson, whose hard work and dedication is inspiring. His brilliant thesis motivated me to finish this one, and his support helped me power through to the end. This thesis, not to mention my degree, would not have been possible without all of you.

Abstract

Glioma is a cancer which begins in the glial cells within the brain. The presence of glioma tumors within the brain can cause a wide variety of symptoms, e.g. seizures, headaches and nausea. The analysis of these tumors is a long and tedious process yet it is essential in determining the correct line of treatment for patients whose life expectancy ranges between a couple of years to a matter of months. Optimizing the process of diagnosing these tumors is of great interest to the medical field. Furthermore, recent studies present new ways of categorizing these tumors by analyzing the methylation type rather than grade and glial cell of origin. A possible way of analyzing glioma tumors is found through the use of Raman spectroscopy. The Raman spectra of the tumors contain information about the vibrations within the molecules of the tumor material.

Machine learning is a technique which has helped in analyzing non-trivial patterns and automating tasks previously thought impossible to perform with computers. The technique utilizes data to form models which have been successful to the point of outperforming their human counterparts. It is evident that the models can perform well in situations where tremendous amounts of data is available. Within cancer research, the focus is on qualitative data gathering rather than quantitative. This is because data gathering is often expensive and lacking due to a limited number of patients available for study.

In this thesis, we explain the process of analyzing the spectra extracted from the tumors of glioma patients. The analysis is performed by sorting the spectra into different groups which maintain minimal variance among the different frequencies within the grouped spectra. This is done to separate tumor spectra from spectra extracted from non-tumor material which may have been present during scanning i.e. plastic, blood, necrotic tissue etc. We utilize machine learning methods to group and examine the samples in detail. We also validate the analysis and preprocessing by creating a model in an attempt to classify the tumors according to the new categories based on the methylation types. Our findings and conclusions as to how these methods can be utilized further for improved results are also presented as a conclusion to this thesis.

Chapter 1

Introduction

The mammalian brain contains so-called neurons and glial cells. Historically, it was believed that the brain contained ten times as many glial cells as neurons, but recent studies suggest the number of neurons is equal to the number of glial cells [1]. Glial cells were also previously thought to be insignificant in terms of the brain's computational functionality, only lending structural support to the neurons. Recent studies have disputed this and suggest their contribution to the nervous system is greater than once thought, though their actual function is still a research question. Glioma is a type of brain cancer which manifests within the glial cells and disrupts brain functions. The survivability of the cancer is extremely poor, with a life expectancy of a few months (without treatment) to a few years depending on the patients health, the tumor type and cancer severity; rarely do patient's survive for longer than five years [2, 3, 4]. Gliomas are categorized depending on their glial-cell of origin. There are four main types of glial cells (also called neuroglia or simply glia): oligodendrocytes, astrocytes, ependymal cells and microglia. Oligodendroglioma originates from oligodendrocytes, astrocytoma from astrocytes and ependymomas originate from ependymal cells. Furthermore, astrocytoma-types may develop into glioblastoma multiforme (GBM), the most aggressive form of brain cancer; this may even communicate with microglia to increase tumor growth [5]. It is also possible for GBM to develop from other brain cells [2]. This cancer is particularly aggressive, due to its quick reappearance in the brain, only a short period after surgery [3]. The heterogeneity of GBM-cells further complicates the healing process, due to poor response to targeted treatments [6].

The World Health Organization (WHO) has defined four levels (or "grades") of cancer severity used to describe the cancer aggressiveness and tumor growth. Grades I and II are considered low-grade and grades III and IV are considered high-grade. Glioblastoma is categorized as a grade IV cancer [4, 7]; these grades are used to determine an appropriate prognosis and line of treatment. A study by Vi-

gneswaran et al. [7] suggests these grades could be divided further to better describe the features of the tumors. This suggestion is also supported by Hirose et al. [8]. Ceccarelli et al. [9] introduce alternative subdivisions of these classes, which show promise in expanding knowledge about glioma tumors and aid in treatment selection. Such evaluations require in-depth knowledge about the tumor tissue in addition to further examination of it, which may last for weeks after the tumor extraction. Ceccarelli et al. define the subdivisions by six distinct classes, labeled LGm1-6. Their analysis showed IDH mutations in LGm1-3; as the name suggests, IDH mutations refer to mutations in the IDH1 or IDH2 genes. These mutations are shown to be significant in a variety of cancers, including glioma [10]. These subdivisions are reinforced by the results produced by Vigneswaran et al. The process of determining a prognosis and a line of treatment using the subdivisions shows great promise in improving patient outcome.

This thesis is the result of a project whose purpose is to optimize the categorization process, based on a deep learning model capable of predicting tumor-types in a matter of minutes. The project relies on tissue from tumors extracted from 45 patients and scanned using Raman spectroscopy. Raman spectroscopy was introduced by Chandrasekhara Venkata Raman and measures the vibrations of molecules by spectral analysis. This method can be executed fairly quickly and can provide chemical information from the spectral light. A laser emits a ray unto the tumor tissue, causing the energy level of the molecules within to change, which in turn changes their vibrations. These vibrations are gathered by the instrument and provide information regarding the molecular properties of the material [11, 12]. These spectra is the data which the model uses as training and testing data. The choice of using Raman spectra in this way is due to the method's success in previous studies of Raman spectra using machine learning [13, 14]. The use of Raman spectra is further motivated by Liu et al. [15], whose work show promise for deep learning models trained on raw Raman spectra. The advantage of this method in the context of multilabel classification seems considerable, when compared to other machine learning methods such as Support Vector Machines, Random Forest and K-nearest neighbor [15].

This thesis aims to analyze the spectra extracted from all patient samples in an attempt to automate outlier detection.We examine the samples by applying statistical methods, hierarchical clustering and K-means clustering; this produces subdivisions of spectra and identifies outliers. These results are compared to the results of a criterion for finding outliers in the data (defined by the data provider). The method most suitable for this purpose is subsequently used to remove the outliers. Following the removal of the outliers, we present a pre-processing pipeline which

will be used to prepare the data for machine learning applications such as Artificial Neural Networks or Random Forests. The features which best divide the data into the six LGm classes are extracted. These features drastically reduce the size of the spectra which are analyzed for prognosis, which in turn reduces the examination time. We thus aim to provide a clear way of preparing Raman spectra for machine learning applications and provide the most important features those spectra consist of. Suggestions for and discussion of how these methods may be improved, which alternative methods could be tested instead and possible limitations of this project are also presented for future consideration.

The thesis is structured as follows. Chapter 2 presents the preliminary background for the statistical methods used in the project, along with the necessary mathematical definitions by which these methods are defined. Among these, we discuss the notions of mean, standard deviation and analysis of variance (ANOVA). Understanding the underlying definitions and consequences is necessary to validate and confirm the results. Therefore, the chapter also presents the definition of supervised and unsupervised learning. The formal definitions of K-means clustering and hierarchical clustering are presented. In Chapter 3, we discuss the analysis methods in detail, to give further understanding of the data on which this project is based. The chapter begins by introducing the concrete shape of the data. Feature selection is applied to the data and the results are examined. The majority of this chapter is based on the visual analysis of the outlier detection. This is done by applying the statistical methods and the clustering methods to the samples. The results of each method are analyzed in comparison to the criterion defined by the data provider. This is done in great detail to form an argument for, or against, the method under analysis. The chapter ends by removing the outliers using the optimal method and performing feature selection once more on the data devoid of outliers. In Chapter 4, we present our suggestion as well as arguments for the pre-processing pipeline to prepare the data for machine learning. A Neural Network is created and trained on the curated data. The performance of the architecture is measured and presented. The thesis is concluded in Chapter 5, where we discuss improvements to our methods and suggestions for alternative solutions to the problem at hand. These suggestions extend to the feature selection and pre-processing stages for future study.

Chapter 2

Preliminaries

In this chapter we review the concepts on which this thesis is based. We first cover the statistical concepts and unsupervised methods necessary for understanding the analysis performed in Chapter 3. We then proceed by reviewing common concepts and specific methods within machine learning which is the central theme in Chapter 4.

2.1 Statistics

In this section we discuss the basic statistical concepts required for understanding the methods used in this thesis. We first explain the mean and the standard deviation. The mean is a value used to describe the average value of a population. A population is the term used to describe the complete collection of elements in some context e.g. all people alive, all numbers in an interval etc. The mean is an important concept in statistics as it is often used as a characteristic of the elements found in the population under analysis when its elements are quantitative [16]. The mean is calculated by the sum of each element divided by the number of elements in said population. The mean μ of a population of n numbers $L = \{L_1, ..., L_n\}$, is calculated as expressed in formula (2.1).

$$\mu = \sum_{i=1}^{n} \frac{L_i}{n} \tag{2.1}$$

The mean of a population is often used in association with the standard deviation. The standard deviation is the square root of the variance of that population. The variance is an expression for the scaled summed squares of differences from the mean of the entire population. Calculating the square root then produces a value expressing the dispersion of elements within the population around the mean. The variance is calculated by measuring the summed squared distance between each el-

ement within the population and the mean, divided by the number of elements in the population to scale the sum. In the case where the entire population is impossible to analyze or unknown, samples are extracted from the population (i.e. subgroups of elements randomly taken from the population). The sample variance changes slightly form the population variance; it divides the summed squares of differences by the number of elements in the sample subtracted by one. Subtracting the original denominator by one is called "Bessel's correction". The correction is based on the fact that, if the population mean is unknown (as is often the case when samples are gathered), then the mean used in calculating the variance will only be an estimation. Subtraction by one is performed to avoid bias towards the sample mean and get an unbiased estimation of the population variance [17, 18]. The standard deviation σ of a sample is thus calculated as expressed in formula (2.2).

$$\sigma = \sqrt{\frac{\sum_{i=1}^{n}(\mu - L_i)^2}{n-1}} \qquad (2.2)$$

2.1.1 The standard deviation test

The mean and standard deviation can be used to detect outliers in a sample of data points drawn from an unknown population. The Gaussian distribution (also called the normal distribution) is used in association with the mean and the standard deviation. If the frequency which elements appear within a sample are more likely to be close to the mean than far away from it, we say that the elements within that sample are normally distributed. If an element differs from the mean by more than three standard deviations, the possibility of that element not belonging to that distribution is extremely high. Such elements, which likely do not belong to the population, are called outliers. The method which detects outliers by measuring the distance between each element and the mean is referred to, in this thesis, as the standard deviation test (SDT). The test assumes that elements within the collection are normally distributed with some mean μ_c and some standard deviation σ_c (where c is the collection from which they are measured). By computing the z-score of the elements, the data is transformed into a standardized form through standardization. Z-score standardization subtracts the mean from all elements in the collection and divides the difference by the standard deviation, as expressed in equation (2.3) [19].

$$\frac{L_i - \mu_c}{\sigma_c} \qquad (2.3)$$

Following standardization, the entire sample will have a mean of zero and a standard deviation of one. Each element in the sample can then be measured using the standard deviation (one) as unit; outliers can then be discarded from the sample

by removing elements which have an absolute value of 3 or higher.

2.1.2 The interquartile range method

An alternative method suited for outlier detection is the interquartile range method (IRM). IRM is based on analyzing the sample by its median, which is the center element of the sorted sample. It is applied by sorting the sample elements in ascending order and organizing the sample into four percentiles, each percentile containing 25% of the sample. These percentiles are called the q_{25}, q_{50}, q_{75}, q_{100} percentiles. Two consecutive quartiles center around 50% of the sample contents, the 50% in the center is referred to as the interquartile range. IRM requires two values from the sample: the highest value of the 25th percentile and the highest value of the 75th percentile. The former value is gained by taking the biggest value of the q_{25} first elements from the sorted collection, where q_{25} is the first 25% of the number of elements in L (calculated by $0.25 \cdot n$). The latter value is gained in a similar fashion, with the exception that the highest value is taken from the first 75% of the sorted data. Two *cut-off* points are then defined, by multiplying each of the two values by a constant k (which is called the *cut-off* constant). Elements can then be labeled as outliers if those elements fall below the lower *cut-off* point or above the higher *cut-off* point. [20, 21, 22].

2.1.3 Analysis of variance

The analysis of variance (ANOVA) is a method for statistical analysis developed by Ronald Fisher to analyze the difference among sample means in a collection of samples. It is based on the null-hypothesis stating that the sample means of two or more samples are the same. The analysis then yields a F-value and a p-value which are used with the F-distribution to accept or reject the null-hypothesis. The analysis assumes the population samples drawn are normally distributed and that the samples are independent of each other. It also assumes the standard deviations and variances are roughly equal among the samples [23].

The analysis is performed by calculating the mean of each sample. The summed square of differences from each mean are then calculated for their respective sample, the result is then subtracted by the squared sum of the elements within the sample divided by the number of elements in said sample. This calculation for sample S is formally expressed in equation (2.4), where μ_S is the mean of sample S.

$$\sum_{s \in S}(s - \mu_S)^2 - \frac{(\sum_s^S s)^2}{|S|} \tag{2.4}$$

This is performed once for all samples drawn from the population, the results are then summed together into a sum of sample sums (SS). The calculation is also performed once on the total collection of all elements from all samples, the result is stored in the total sum of sample sums (SST). The total sum of squares is the sum of SS and the sum of squared distances from each sample mean to the total mean (SSM). SSM is therefore calculated by subtracting SST and SS. The analysis also requires divisions by two values called the degrees of freedom. They are calculated as follows: d_1 is the number of samples subtracted by one and d_2 is the number of elements in the total collection subtracted by the number of samples. The F-value is calculated by a fraction of two fractions. Let K_1 be the fraction $\frac{SSM}{d_1}$ and K_2 be the fraction $\frac{SS}{d_2}$, the *F-value* is defined as expressed in formula (2.5).

$$F = \frac{\frac{SSM}{d_1}}{\frac{SS}{d_2}} = \frac{K_1}{K_2} \tag{2.5}$$

The quotient yielded by the fraction in formula (2.5) can then be inserted into a pre-calculated table of the F-distribution using the degrees of freedom to yield the p-value. A small p-value (i.e. lower than 0.05) indicates that the null-hypothesis may be rejected with relative certainty whereas a high p-value indicates the null-hypothesis holds and should be accepted with relative certainty [24].

2.2 Machine Learning

Machine learning is the practice of computing models for relationships between sets of data. The field has garnered significant interest within academia and industry alike due to the promising results in applications for which deterministic algorithms have proven difficult or impossible to make. Examples of such applications are computer vision, natural language processing and personalized advertising, to name a few [25, 26, 27]. There are two main paradigms for learning: Supervised learning (using labeled data to approximate models) and unsupervised learning (finding patterns within the data itself).

Models are used to great length within many scientific domains. In the context of machine learning, a model can be seen as a data structure made out of constant parameters combined with an algorithm which utilizes the data structure to produce predictions given an input vector (the input can also be in the form of a multi-dimensional matrix).

The model can be represented mathematically as a collection of structures in the form of vectors or matrices, the elements of which are referred to as parameters. A model can consist of learnable parameters θ and non-learnable parameters (often

generated by stochastic initialization if used). The model computes a function f to yield a prediction y by applying the algorithm to the parameters given an input example x (which can be a vector or a matrix) drawn from the data set X. Let the dimensionality of the input x be equal to the dimensionality of θ. An example of a model prediction, where the algorithm produces predictions through addition, is given by formula (2.6).

$$y = x_0\theta_0 + x_1\theta_1 + ... + x_n\theta_n \qquad (2.6)$$

Machine learning then, is the practice of changing (also known as tuning) θ by introducing small changes to the elements within θ. This is done to minimize a loss function which computes the error (or loss) given y. The process of changing θ is known as the training process and is central to machine learning.

In the training process for supervised learning, the data gathered for the model is separated into three sets. These sets are referred to as the training set, validation set and test set. They are randomly collected samples from the common data set such that the intersection between any two sets is empty. The purpose of the training process is to train the model on the training data and use the validation and test sets as a means to validate the model performance on data not encountered during the training process. Supervised learning requires that the examples used have a label which the model tries to predict (data which possess labels are called labeled data). We say that a model generalizes well to the data if the training process allows the model to perform well on unseen data. If the model manages to perform well on the training set but fails to generalize, the model is said to overfit to the data.

Unsupervised learning is a learning paradigm which does not rely on the use of labeled data. Instead, the paradigm focuses on organizing the data in a way that minimizes the loss function. Predictions can then be performed by evaluating the way the data has been organized by some method related to the problem context. The problem context is usually framed by two problem categories. These categories are regression and classification. Regression is the task of predicting continuous values given either continuous or discrete data i.e. predicting stock prices given information about the current economical situation or predicting the number of patients in a hospital during a pandemic given the density of the population. Classification aims to group different examples into categories (or classes) i.e. predicting whether an image contains a dog or a cat or which category a given tumor belongs to. Both supervised and unsupervised learning are used in this project.

2.2.1 K-means Clustering

Clustering is an unsupervised learning method whose primary use is in grouping data into sets. In this thesis we consider the *K-means* clustering algorithm. The following is a formal definition of *K-means* clustering as defined by MacQueen [28]. Given a set E_n of *n*-dimensional points (where $n \in \mathbb{N}$) and a desired amount of partitions k of E_n, partition the elements of E_n into k sets. The partitions are stored in a superset S such that $S = \{S_1, S_2, ...S_k\}$. The partitioning of E_n is performed by randomly initializing k *n*-dimensional points as randomly selected points within E_n, these are the initial clusters. We define the set of clusters V with elements v, where v_i is the i:th cluster center and $i \in [1,k] \cap \mathbb{N}$. The partitioning of the elements $x \in E_n$ into their respective partition S_i is performed by computing the closest cluster center for all elements in E_n. Let T_i where $i \in [1,k] \cap \mathbb{N}$ be the set of elements $x \in E_n$ such that the distance from the element to the relevant cluster center is minimal; T_i is defined by formula (2.7).

$$T_i = \{x : x \in E_n | (|x - v_i| \leq |x - v_j|)\}(j \in [1,k] \cap \mathbb{N}) \tag{2.7}$$

For centers that share equal distance to any given x, the cluster with the smallest index is chosen as the containing set. This is performed by iteratively defining S_i as the intersection of T_i and the points which are not in any prior partitioned sets i.e. for S_j where $j < i$. This is denoted by the set complement S_i^c for all elements not in S_i. Let S_1 be defined by T_1, then the partitions $S_i \in S$ for $i \in [2,k] \cap \mathbb{N}$ are defined by formula (2.8).

$$S_i = T_i \cap \bigcap_{j=1}^{(i-1)} S_j^c \tag{2.8}$$

A consequence to this definition is that outliers have a potential to drastically change the quality of the clustering outcomes [29]. To remedy this and the stochastic nature of the initialization process, the method is run several times on the same dataset, yielding the optimal solution from those runs. This does not guarantee the best solution for the problem, but the solution is approximated. The problem *K-means* clustering attempts to solve is proven to be NP-hard [29, 30] but the algorithm itself has a time complexity of $O(n^2)$ [31].

2.2.2 Hierarchical clustering

Hierarchical clustering is a deterministic clustering method. Each cluster formed is based on the entire dataset, in contrast to *K-means* which approximates clusters

by performing small changes to the cluster centers. The method produces clusters by iteratively combining the closest clusters according to the given linkage criterion (defined in section 2.2.2.2). The two primary strategies for forming clusters are agglomerative and divisive. Agglomerative clustering initializes one cluster for each data point and combines them in a hierarchy according to the linkage criterion until all clusters are part of the hierarchy. Divisive strategies initializes one universal cluster for all data points and proceeds to separate the points into distinct clusters according to the linkage criterion. The method proceeds until all data points are separated to their own cluster within the unifying hierarchy. The project described in this thesis uses the agglomerative strategy. All strategies rely on specific distance metrics and linkage criteria [32].

2.2.2.1 Distance metrics

Let u and v be vectors of the same dimension $n \in \mathbb{N}$. The *Euclidean distance* (also called *L2-distance*) metric can be used to measure distance between the vectors in Euclidean space. The *Euclidean distance* between u and v is defined by formula (2.9).

$$d(u,v) = \sqrt{\sum_{i=1}^{n} (u_i - v_i)^2} \tag{2.9}$$

The *Manhattan distance* (also called *L1-distance*) metric is also a viable alternative, if the distance is to be measured in blocks. The distance is akin to finding a shortest path among blocks and is therefore calculated as expressed in formula (2.10).

$$d(u,v) = \sum_{i=1}^{n} |u_i - v_i| \tag{2.10}$$

Cosine similarity measures similarity between vector angles and suits situations where certain vectors are expected to be similar. Should the vectors be sizable in terms of dimensionality, this method will yield varying results, especially if the elements have vary significantly in each dimension. It is calculated as expressed in formula (2.11).

$$d(u,v) = \frac{\sum_{i=1}^{n} u_i v_i}{\sqrt{\sum_{i=1}^{n} u_i^2} \sqrt{\sum_{i=1}^{n} v_i^2}} \tag{2.11}$$

2.2.2.2 Linkage Criteria

In order to measure distance between clusters it is essential to know between which points the distance should be measured, since clusters often consist of several points. Linkage criteria describe the method for determining how the distance metric will be applied. In this project, we use the library SKlearn and the already defined methods within it to perform our analyses; the following criteria are therefore the only focus for this subsection. SKlearn defines four criteria in the documentation: Single linkage, complete linkage, average linkage and ward linkage [33]. Depending on which criterion is applied, the results may differ considerably.

Single linkage goes through each pair of clusters measuring the distance among all points within one with respect to the other. The distance between these clusters is determined to be the distance between the two closest points. Let U be the elements in the first cluster and V be the elements of the second. The distance between the first and the second cluster is defined formally in formula (2.12).

$$d(U,V) = \min_{(u,v)\in U,V}(d(u,v)) \tag{2.12}$$

Single linkage tends to produce trivial results, forging a hierarchy in a chain where individual elements slowly merge with the bigger cluster. In contrast, complete linkage considers the largest distance between two points for every pair of clusters. The distance between two clusters then becomes the distance between the points which are the furthest apart, formally expressed in formula (2.13).

$$d(U,V) = \max_{(u,v)\in U,V}(d(u,v)) \tag{2.13}$$

By considering the largest possible distance between two clusters, this criterion bypasses the setback of single linkage, allowing more clusters to form before merging into one unifying cluster.

Average linkage calculates the average between all elements for every pair of clusters and merges the ones possessing minimal average distance. It is formally described by formula (2.14).

$$d(U,V) = \frac{1}{|U||V|} \sum_{u\in U} \sum_{v\in V} d(u,v) \tag{2.14}$$

Ward linkage represents distance by how much the summed square would increase by merging them. The method aims to merge the clusters such that the within cluster variance is minimal. Let c_a be the center of cluster a, then ward linkage is expressed formally by formula (2.15) [34].

13

$$d(U, V) = \frac{|U||V|}{|U| + |V|} ||c_U - c_V||^2 \qquad (2.15)$$

2.2.3 Feature Selection

In many cases, the data available contains numerous features; e.g. different frequencies on a spectrum, which often helps to build sufficient classifiers, as the model may find non-trivial patterns among the features. To avoid expanding the dependence on large datasets and to minimize the computation time, it is often necessary to rid the data of certain features. Ideally, the features selected for removal are those which provide the least information or are completely uncorrelated with the subject under study. An example for such a feature would be the color of someones clothes correlated with the chances of said person seeing a squirrel on that day. In other words, features are removed if they possess minimal correlation to other features or lack correlation entirely [35]. Features that possess the necessary expressive information are not always trivial, and there are several ways in which they may be found. In this project we exclusively use one form of feature selection with the SKlearn library. The SelectKBest method is a method which ranks features by their significance according to some scoring function. In this project, we use the f-classif method to score the features in the data set. The method computes the F-value using ANOVA for each feature in the data provided, the features are then sorted according to the F-value after which, SelectKBest returns the k features with the highest score.

2.3 Deep Learning

Deep Learning (DL) is part of machine learning and concerns the use of massive models. DL is commonly used in association with Artificial Neural Networks (or simply Neural Networks) which have been used to great success in classification and regression tasks alike. In this section, we review the preliminary methods central to Neural Networks in the context of DL. The concepts of activation functions, layers and optimizers are covered in context of what the project requires.

2.3.1 Neural Networks

Neural Networks are machine learning models which have been used to great success during the 21st century; in no small part due to the increase in computational power over the past decade. With the use of Neural Networks, several fields including Natural Language Processing, Encoding and Image classification have undergone revolutionary leaps in performance regarding optimization due to the predic-

tive power of these networks [36, 37, 38, 39]. At the same time they are heavily criticized for their complexity, yielding a structure much more akin to a so-called *"black box"* than a reliable and deterministic method for prediction. This complexity is due to numerous different structural typologies available at present and an awesome number of learnable parameters [40]. A consequence of this is hard skepticism regarding the correctness of their functionality within practical use. While these models have shown great promise when compared to their human counterparts, the question remains whether or not perfect performance can be yielded from the constructed models.

A Neural Network consists of a set of learnable parameters W_n, $n = 1, ..., k$ for a model possessing k layers. These parameters are commonly referred to as weights and are matrices with arbitrary dimensionality, with a set number of parameters for each element in the input x. The first set of weights have one dimension set to the shape of x and the other shapes are chosen according to the size of the layers specified by the user. The last set of weights W_k has the size of the expected output signal i.e. the number of different categories available in the context of classification. The layers denote the size of the different shapes the input is transformed into as the input propagates through the architecture. The input is propagated through the architecture via the dot product of the weights and the layer signals, yielding a new vector of shape l_n. Layers can also be convolutional, meaning they are multi-dimensional structures which can be used in the context of image classification and Natural Language Processing, where input can be read in sequences, rather than giant data structures. This is managed by initializing smaller kernels which are able to compute signals from the input by only observing the defined size, they move over the entire input by steps called strides after which a pooling layer is used to summarize the final layer signal. Between each transformation, an activation function is used to transform the signal further in a non-linear fashion. Each layer transformation f_n is then the yielded signal from the activation function given the dot product between the current and preceding layer. The signal of layer l_i where $1 < i \leq k$ is then the result of the activation function σ of the dot product of the preceding layer signal l_{i-1} and the weights W_i. This layer function is denoted by the output of the nested function call of all functions $f_0, f_1, ... f_i$ of input x as expressed in formula (2.16) [41].

$$f_i(f_{i-1}(...f_1(x))) = l_i = \sigma(W_i \cdot l_{i-1} + b_i) \tag{2.16}$$

The variable b_i is the bias term for the activation. Its inclusion allows the activation curve to be moved along the x-axis. This shift in position of the activation allows the model to further change its own behavior through the learning process.

It avoids bias towards the y-intercept of the activation function.

2.3.2 Activation functions

Activation functions are used in neural networks to transform the input in a non-linear fashion. The function can be any function on numerical elements, the only requirement is that it must be derivable for all possible inputs. The functions usually transform the signal to be in a certain interval such as the hyperbolic tangent function (tanh) or the sigmoid function σ. The sigmoid function was originally used due to the similarities with the activation of biological neurons. The "s"-shaped curve of the function transforms any signal to the interval $[0,1]$. It is comparable to tanh, which transforms signals into the interval $[-1,1]$. The functions are formally expressed in formula (2.17) and (2.18), respectively.

$$\sigma(x) = \frac{1}{1 + e^{-x}} \tag{2.17}$$

$$tanh(x) = \frac{e^x - e^{-x}}{e^x + e^{-x}} \tag{2.18}$$

Choosing an activation function depends on what range the user wants the signals to fall into. Sigmoid and tanh work sufficiently well for many models, giving promising results for many different tasks within DL. One flaw is that they are computationally expensive to calculate. The rectified linear unit (ReLU) is an activation function which is easily computed for many elements without the necessity for significant amounts of computational resources. The ReLU function returns the input itself if the input is greater than zero, and zero otherwise. The derivative of ReLU is similarly efficient to compute, the derivative is one for input greater than zero, and zero otherwise. The function is shown to outperform sigmoid and tanh as activation function in many cases, which has promoted its use in several applications. The drawback of ReLU is the derivative of 0 for signals of zero and below. The derivative is used during the training process to introduce changes to the model. With ReLU, the activation signal will become zero if the signal is smaller than zero. The neurons which suffer from this problem are referred to as "dead", since the weights used for their activation always bring the signal to or below zero. A possible fix for this is the leakyReLU function, which introduces a slight slope to the ReLU curve for values below zero. The ReLU function may then be defined through the leakyReLU function with a slope of zero for signals below zero. The derivative of leakyReLU then becomes one for values greater than zero, and a small real number for values below zero [42, 43].

The final activation function introduced in this section is the softmax function.

Softmax is a method which transforms the signal in the output into a probability distribution i.e. scales the signals according to the maximum element and transforms the data to have a sum of one. This is done using Euler's constant e as base, dividing e raised to the power of each element in the input signal by the sum of all exponents. This is formally expressed in formula (2.19) [44].

$$\sigma(x)_i = \frac{e^{x_i}}{\sum_{j=1}^{k} e^{x_j}} \qquad (2.19)$$

2.3.3 Regularization

Regularization methods are used during the training process to aid in generalization for Neural Networks. One such method is dropout, which assigns a dropout rate to specifically selected layers. Dropout randomly reduces signals of individual neurons in the selected layers to zero which prevents the model from enforcing connections which become heavily affiliated with certain types of predictions. This is especially important in large architectures where layers can consist of hundreds of neurons where strong reinforcements are easily established [45]. Gaussian noise may also be added to all signals in any layer to shift the signals in them sporadically. However, this method requires some knowledge about the range of the signals within the layers, as large additive noise can remove any necessary information from the input which affects the gradient significantly. The model will learn to reduce dependency on noise during training, provided the noise is not "destructive". For example, adding Gaussian noise drawn from a normal distribution with a standard deviation of five to signals returned by the sigmoid activation function. This will shift the distribution of signals which removes valuable signal information. Batch normalization is a regularization technique which normalizes the change applied to W_n during training over several batches of input and helps regularizing the model [46].

2.3.4 Optimization

Neural Networks have many usable loss functions depending on context. In the context of classification with multiple categories, categorical cross-entropy is commonly used to measure error between the prediction of the network (usually produced with softmax or sigmoid activations) when the prediction is meant to categorize the input. The cross-entropy loss is calculated as the sum of negative elements of the true label y^t multiplied by the logarithm of the predicted label y. Let k be the number of elements in the output signal y, the cross-entropy loss is formally expressed in equation (2.20).

$$-\sum_{i=1}^{k} y_i^t log(y_i) \hspace{3cm} (2.20)$$

Equation (2.20) measures the entropy between two distributions, entropy being the loss of information between two different distributions. The equation assumes the values within y are elements of a probability distribution, i.e. the sum of the elements within y equals one. The negation of the logarithm is used to bring the elements of the sum to a positive scope. This ensures the loss will be positive, since all elements in y and y^t are in the interval $[0, 1]$. The sigmoid function may also be used in association with cross-entropy, as the values will be transformed into the zero-to-one interval. Other activation functions such as tanh and ReLU run the risk of bringing elements in the sum to the negative scope or undefined (as the logarithm is undefined for values less than zero) [47, 48].

The computed loss between the data labels and the predicted labels is then used by the optimizer to change the learnable parameters. The backpropagation algorithm calculates the partial derivatives of the computed loss with respect to each learnable parameter. The collection of the derived parameters are called the gradient. The gradient is scaled by the learning rate (usually a value less than 0.01) defined in the optimizer, this allows for small changes to each parameter which allows the model to approach the minimum of the loss function at a speed proportional to the learning rate. Using the gradient in this way is called gradient descent and it is the common method of learning all optimizers use. Adam is an optimizer introduced by Kingma and Lei Ba [49] which has proven to be efficient in contrast to other optimization methods such as Gradient Descent, AdaGrad and RMSprop. Adam uses an adaptive learning rate to approach the minimum of the loss function. Adam requires four different parameters for the algorithm to run. These are the learning rate α, stochastic decay rates β_1 and β_2 and a small constant ε used to avoid division by zero for the update equation. The algorithm described by Kingma and Lei Ba also requires two vectors m and v used to describe the "moment" of the gradient and the squared gradient respectively (initialized as zero vectors). The gradient update at timestep t is expressed by the following formulas:

$$t = t + 1$$
$$g_t = \nabla L_t(W_{t-1})$$
$$m_t = \beta_1 \cdot m_{t-1} + (1 - \beta_1) \cdot g_t$$
$$v_t = \beta_2 \cdot v_{t-1} + (1 - \beta_2) \cdot g_t^2$$
$$m_t' = \frac{m_t}{1 - \beta_1^t}$$
$$v_t' = \frac{v_t}{1 - \beta_2^t}$$

18

$$W_t = W_t - \alpha \cdot \frac{m'_t}{\sqrt{v'_t} + \varepsilon}$$

Each vector at timestep t uses the values for the "moments" at the previous timestep $t - 1$. Each "moment" is then updated using the previous timestep and the stochastic decay rates. Each "moment" vector is normalized by element-wise division of the "moment" vectors and their respective decay rates to the power of t. β_1 and β_2 are initialized to be 0.9 and 0.999 respectively, this ensures that subtraction by one will maintain the relative scope between the "moment" vectors and their corrected counterparts. The parameters themselves are then updated by subtracting the current parameters by alpha multiplied by the decay rate (calculated by the fraction of the "moment" vectors with the ε parameter added to the denominator). The "moment" vectors then give each feature a unique learning rate which accelerates training.

Chapter 3

Data Exploration

Machine learning assumes that the data possess sufficient characteristics to approximate the sample population from which it was extracted. Therefore, we examine the data in an attempt to remove outliers and to determine if the data is sufficient for classification. In addition, in a particular case study, certain tumors have been shown to be heterogeneous [50]. This can be problematic for a classifier, as heterogeneous samples lack in shared characteristics.

In this chapter, we examine the data available to the project. In particular we investigate how the Raman spectra have been prepared, as their processing is essential for analysis. We undergo several steps as follows. First, we describe the mathematical representation of the samples. Since the number of samples is rather small for learning, we explain how each sample may be separated into individual spectra; this separation yields a drastic increase in the number of available training examples. Second, we explain how to balance the data; an unbalanced dataset would likely introduce bias during learning, rendering the model's desired predictive capabilities uncertain. We achieve this by duplicating samples belonging to underrepresented categories in the dataset. Furthermore, this balancing is performed to maintain majority and minority categories, thus retaining some distributional information from the original dataset. The main goal of our analysis is to analyze the data using different methodologies for detecting spectra which have been altered due to non-tumor material affecting them (henceforth called outliers). As a starting point for our analysis, we have defined the frequency criterion. The criterion is used to separate tumor spectra from outliers in each sample. The outliers captured by this criterion are compared to outliers detected by other outlier detection techniques such as the Standard Deviation Test (SDT) and the Interquartile Range Method (IRM). The unsupervised machine learning methods K-means clustering and hierarchical clustering are also used to detect outliers in each sample. The results from each method are then compared to select the one which best separates

outliers from the tumor spectra, after which the data is curated by that method.

Another point of interest in this project is the identification of representative frequencies within the spectra. Each spectrum belongs to a tumor which can be categorized by six different categories. Our hypothesis states that certain frequencies should be sufficient in determining which category the tumor belongs to. Feature selection is used for this purpose, representing each frequency within the spectra as distinct features. However, in order to extract such features reliably, the data must be devoid of outliers. Should outliers exist within the dataset, the features given by the methods used will be influenced by the outliers. To prepare for this, the data is plotted for visual inspection. It is confirmed by the data provider that the majority of samples include outliers. These outliers are influenced by a variety of other materials found on the tissue's surface, e.g., spectra of blood drops, plastic which may be reflected form underneath thin tissue or necrotic tissue, which is shown to affect the spectral signal. Using the extracted features, a model can be trained on the data faster, this is essential, as many machine learning methods require a significant number of computing resources and data. The features are extracted before and again after the removal of problematic spectra. This is done to compare the impact of the outliers in feature selection. We expect the features yielded to vary significantly for different subsets of the available data. Feature selection is suited for cases where different subsets of the data can be described by the same same set of features extracted from part of the data set. In this particular case, should the extracted features vary tremendously among different subsets, the model may accidentally be trained to disregard features relevant for unseen data. This would yield a model unfit for use in a medical environment, where the predictions must rival that of trained professionals.

3.1 Data Representation

The data consists of the Raman spectra extracted from the tissue of glioma tumors from 45 patients. Multiple samples of tissue were extracted from the same patient in some cases, yielding several samples for the respective patient. To maintain separation among the patients, the samples are sorted by their respective patient of origin. This is necessary due to the heterogeneity of each tumor. The data will be separated into three separate datasets. These sets are referred to as the training set, the validation set and the test set. Due to the expected heterogeneity, all datasets will consist of unique patients to avoid scenarios in which the model overfits to a patient's tumor sample. This structure also allows for easier handling of the number of patients in each sample category, allowing for analysis on each category separately from the

others.

There is also large variation with regard to the sample shape within the data. Each sample is a three-dimensional array of shape $(w, h, 1738)$ where w and h are the width and height of the sample, respectively. This formalization is necessary, as width and height have non-zero variance among different samples. The shape is a result of how the tissue was scanned. In each case the tissue was placed inside the Raman spectrometer and scanned successively from side to side. This makes it possible to display each sample as an image, by substituting the third dimension (denoted above by 1738) with a color value denoted by which category the spectra belong to. The number 1738 is constant through all samples and represents the length of a modified Raman spectrum. The spectra has been modified by the data provider; the data consist of spectra resulting from a linear function on the extracted spectra. This is done to omit unnecessary frequencies and allow focus on parts of the spectra which we believe are sufficient for this project. Furthermore, each element inside these arrays is a real number without clear bounds. The largest absolute element found within the complete dataset is 79427.0625. Some values are negative, which is confirmed by the data provider to have significance for the project's purpose. The project aims to prepare these spectra for use in machine learning methods. Predictions should be performed on individual spectra extracted from the dataset. We choose this strategy since each spectrum is independent of all other surrounding spectra, ideally sharing in some characteristics from the other spectra belonging to the LGm category we wish to predict, i.e., one spectrum should describe which LGm category the sample belongs to. There are six distinct LGm categories as defined by Ceccarelli et al. [9], denoted LGm1 - 6. The model will take as input one vector of shape $(1, 1738)$ and produce one vector of shape $(1, 6)$. This strategy is inspired by Liu et al. [15], who managed to achieve satisfactory performance by training a model on raw spectra i.e. spectra without pre-processing or outlier removal. Restructuring of the data to represent all samples as a list of spectra rather than 3-dimensional matrices yields a dataset with more than $300,000$ datapoints, which is a sufficiently large dataset for machine learning.

Initially, we choose to examine each sample visually by observing the spectral lines in a graph. This allows us to examine the general shape and visually deduce if any common patterns are present in the samples and identify problematic samples. As expected from analogue measurements, significant amounts of noise are present in each plot. Despite this, many spectra share some general characteristics with a few spikes appearing on a mostly flat spectral line. An example of the plots created for this examination be seen in Figure 3.1.
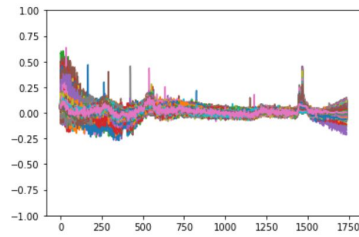
(a) Spectra from patient HF-1293. The rest of the samples available share in this pattern with some deviations
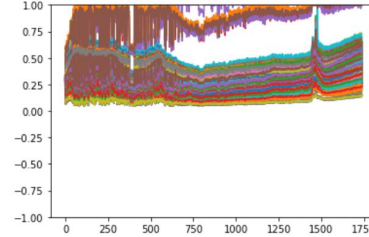
(b) Spectra from patient HF-1887. The frequencies tilt towards the upper part of the plot. The example is decidedly removed from the analysis.

Figure 3.1: Examples of samples drawn from the data: sample HF-1293 displays a common pattern across all samples, sample HF-1887 is removed due to the skewed baseline. The range of the values are normalized between -1 and 1 to more easily display the spectra.

Figure 3.1 shows two collections of spectra, the spectra belonging to sample HF-1293 are shown in Figure 3.1 (a) and spectra from sample HF-1887 are shown in 3.1 (b). The spectra form HF-1293 follow a general pattern visible in the vast majority of sample plots. Sample HF-1887 is an example of one sample which we deem too sporadic for this project, and which we remove, due to the skewed baseline of all spectra in the sample; the data provider agrees with our decision. After visual examination, we can confirm that some characteristics are present, but they are not sufficiently different among the different LGm categories to be classified by a human being in this case. Machine learning is needed to detect precise differences among the samples by observing the spectral lines.

Another reason to remove samples is their size. The analysis we aim to perform requires considerable computational power and memory space. Many of the samples available have a manageable size, as they consist of approximately 3600 spectra i.e. width and height are approximately 60 and 60 respectively. In case the number of spectra in a sample is extravagant, we may simply extract random subsamples from the larger sample and analyze those. However, applying that method at this stage would potentially ruin the form of the samples which is used to evaluate the outlier detection methods in a later section. Fortunately only one sample suffers from this problem. Sample HF-3097, shown in Figure 3.2, shows a concerning number of spikes in contrast to the other samples and is the only sample which requires considerable memory space (the number of spectra exceeds 40000).
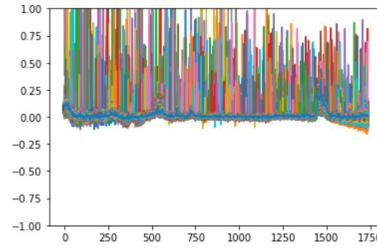
Figure 3.2: Sample HF-3097 from LGm2, the spectra spikes are extremely rare. The range of the values are normalized between -1 and 1 to easier display the spectra.

The values inside the spectra are also considerably bigger than the values found in the other samples. The methods SDT and IQM require statistical constants to be extracted on the entire dataset, including this sample would affect the standard deviation and the mean of the frequencies tremendously (even if the constants were evaluated within the scope of the sample itself). K-means clustering is also an un-supervised machine learning model which can be trained on data before predictions are performed on unseen data. Since the aim is to use the training set for training the model, inclusion of the sample would affect the performance considerably. If the sample was put in the test set for testing, the noise in the signals would affect predictions considerably, which would affect testing accuracy due to what appears to be noise in the frequencies. To avoid these statistical issues and to reduce the computational requirements, the sample is discarded following the data provider's approval.

3.2   Balancing the Data

The model will, as a consequence of the learning algorithm, become biased towards certain predictions if presented with frequent examples of a particular category. As the model encounters frequent training examples, the connections which produce such predictions will strengthen. Overexposure to examples of a certain category will force the model to associate features with that category, redirecting focus from categories for which that feature could be significant. This is why it is important to train models on balanced data. Having a balanced dataset means the number of examples in each category is uniform in the entire training set. Training on a balanced dataset also avoids bias towards data distribution, where certain categories may be predicted more frequently than others simply because the distribution was used in training. The initial data suffers heavily from this problem. Training on the data would result in a model which produces frequent predictions for the majority category (the category which has the most spectra) and performs inconsistently for

the other categories. The initial data distribution is shown in Table 3.1.

Category	LGm1	LGm2	LGm3	LGm4	LGm5	LGm6
# Of samples	5	11	4	10	11	4
# Of spectra	37319	71846	31931	50660	62256	20176
Percentage	14%	26%	12%	18%	23%	7%

Table 3.1: The distribution of data in the initial dataset after removing the problematic samples.

Table 3.1 shows the categorical separation in the data, the header row shows the labels of each category. The first row shows the number of samples belonging to each category, these are the tumors which will be analyzed. The second row displays the total number of spectra across each category; these must be considered for balancing. Note the equal amount of samples in LGm3 and LGm6, but the difference in number of spectra within them. This is due to the varying size of all samples drawn from the tumors. Some samples share the same size, however the important fact is that the samples lack a uniform shape, which must be considered during the analysis. The last row shows the percentage each category makes of the entire dataset. Initially, LGm2 is the majority category while LGm6 is the minority category, consisting of only 7% of the entire dataset.

Before the data is balanced, the testing data is selected and separated from the rest. This is done by separating at least one patient and all their samples from the rest of the data. This way, we ensure the possibility to test if the model develops bias towards the patients in training and if the patient samples are heterogeneous with respect to the other samples of the same category. Samples are chosen with the criterion that approximately 30% of each category is represented in the test set. Balancing the categories which contain less elements by a factor larger than or equal to two compared to the majority category (LGm2) is done by repeating the spectrum in each sample by that factor. This method does not perfectly balance the data to have a uniform distribution of categories, but it does make the underrepresented category frequent enough to circumvent the issue of unbalanced datasets. The multipliers for each categories are chosen so as to retain the majority category i.e. LGm2 will remain the majority category after balancing is done. There is also a need for the validation set; the validation set will be used to monitor the models performance on unseen data during training. The samples for this set are chosen such that one sample from each category is allocated to the set. The separation of the entire dataset into three distinct sets is arbitrary and so can be performed automatically. However, we choose to perform this separation manually to maintain consistency in this analysis. The resulting separation is shown here as it is the training set from which

the features are extracted in this project. We discover that the results will differ slightly depending on which samples are chosen for which set. The distribution of all datasets is shown in Table 3.2.

Category	LGm1	LGm2	LGm3	LGm4	LGm5	LGm6
# Training	17689	47602	37557	30180	33396	9376
# Validation	3600	4096	3600	4096	4096	3600
# Test	14945	20140	11296	16384	24764	7200

Table 3.2: Distribution of the three datasets

Table 3.2 shows the distribution of the different datasets used in this project. The training set is then balanced exclusively. This is not required in the test set or the validation set, since they will have no direct effect on how the model is developed through training. It is also important that the validation and test sets are not uniform, since it will prove whether the model can generalize to different prediction distributions. The training set is balanced by replicating each spectra in every patient of the categories which are under-represented. The number of sample replications per category can be computed by the following method. Let m be the LGm category which contains the majority of spectra in the set and $|LGm_n|$ be the number of spectra in LGm category n. The number of replications for each category can then be computed by $\lfloor \frac{|LGm_m|}{|LGm_n|} \rfloor$. The distribution of the training set after applying the replication method is shown in Table 3.3.

Category	LGm1	LGm2	LGm3	LGm4	LGm5	LGm6
# Training	35378	47602	37557	30180	33396	46880
Percentage	15.32	20.6	16.26	13.07	14.46	20.29

Table 3.3: Distribution of the testing data following balancing

As is shown by the last row in Table 3.3, the data does not have a uniform distribution as LGm2 is still significantly larger than LGm4. However, the important thing is that the distribution is better balanced relative to the original distribution. The biggest difference between the categories is by approximately seven percent. We assume this distribution is good enough and proceed to the next step of the analysis.

3.3 Feature Selection and Visual Analysis

Following the balancing, the first step in the analysis is to find the frequencies which best describe the data with respect to the different categories. Each number in the

spectra is a frequency at which the scattered light is gathered. This number is expected to be sufficient for predicting the categories of the tumor-tissue. We assume that, to sufficiently categorize the spectra into the categories, only certain frequencies are required. For this reason, the most significant features are extracted with SelectKBestfeatures [33], which is given the f-classif method for ranking the features in order of their significance. Following this step, we may pick any arbitrary number of features by extracting them in the order given by f-classif. The 70 best features are extracted from the training set in which there are outliers present still. The features are displayed in Appendix A. The extracted features show that regions of interest do exist on the spectra. This can be seen by the integers which have a successive difference of one, suggesting that the region of interest exists somewhere in specific parts of the spectra. It is worth noting here that the features selected might be correct, provided the amount of outliers is sufficiently small to be ignored by the feature selection method. Due to this uncertainty, the data will be separated from the outliers and feature selection will be performed a second time at the end of this section.

All data is subject to this analysis as all samples must be curated before the model can be trained. In the methods where statistical constants must be calculated, the training data is used, this avoids bias towards the other datasets whose primary purpose is to evaluate the model. The goal of the analysis is to find a uniform criterion which each spectrum must fulfill to be considered *clean*. Spectra which fail to satisfy this criterion will be discarded from the project entirely. In this section the methods of analysis used are described and their results examined. The section begins by examining the frequency criterion, which is a confirmed criterion all spectra must satisfy to be considered "clean". This criterion was provided by the data provider. SDT and IRM are compared to the frequency criterion for validation; these are deterministic methods that rely solely on the values found within the data and are commonly used to detect outliers in data. K-means clustering and hierarchical clustering are then performed on the data in the attempt to capture potentially complex patterns within the data. These methods are specifically designed to allow for grouping of data based on the similarities between data points within the dataset. The section ends by selecting the method which best detects outliers; this method is then added to the pre-processing stage, i.e., all samples must be curated using this method before they can be used by the machine learning model. In the following figures, the yellow parts represent spectra which the the method in question labels as tumor spectra. The darker color represents outliers.

3.3.1 The frequency criterion

The frequency criterion is a criterion specified by the data provider dr. Adrian Lita, for separating outlier spectra from tumor spectra. The criterion states that, should any value of frequencies between 1463 and 1473 of any spectrum be below 5000, then that spectrum is defined to be an outlier. Given that this criterion is defined by the provider, together with the lack of knowledge regarding where outliers may be positioned on the samples, we choose this criterion as the starting point of this analysis. The extracted features in Appendix A include parts of the range on which the criterion is based, which is promising. The range being present in the extracted features can also mean that the outliers work to influence the relationship between the spectra and the categories we want to predict. Hence, the removal of outliers is essential for building an unbiased model. We examine the results of the criterion to gain insight into where these outliers are positioned. The criterion is confirmed to miss some outliers and so it mainly functions as an initial approximation of the areas where outliers are present. An example of this is in sample HF-2849 of LGm3 shown in Figure 3.3.
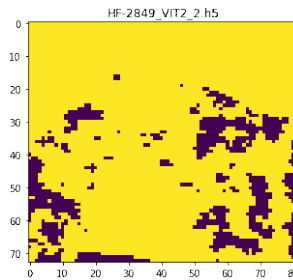

Figure 3.3: Sample HF-2849 from LGm3. The yellow parts of the image represents the tumor spectra saved by the criterion, and the dark spots are outliers. The sample is confirmed to have necrotic tissue present in the upper part which the criterion fails to detect.

The criterion is satisfactory for capturing areas in the lower parts of the sample. However, the upper part of the sample is guaranteed to have spectra from necrotic tissue which is unreliable for describing the LGm Category of the tissue. Necrotic tissue is tissue which has died and cannot yield helpful information through Raman spectroscopy, hence, it must be removed. It appears the criterion is well suited for detecting liquid material on the tissue, since many samples show smaller spots of interest and fail to completely capture larger areas of outliers. This is evident in Figure 3.3, as multiple small spots are detected. This is one of several examples for how the criterion fails to detect all outliers reliably, but in the majority of the samples, the outliers are detected sufficiently well. One such case can be seen in sample HF-868 displayed in Figure 3.4.
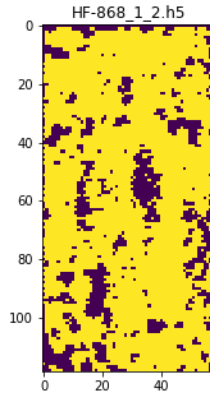
Figure 3.4: Sample HF-868 from LGm1. The areas detected are confirmed outliers.

According to the data provider, the outliers present in HF-868 are sufficiently captured by the frequency criterion. The outliers form as small, sporadic areas on the surface of the tissue. This shape is what the outliers are expected to have in the samples which are known to include them. However, since the frequency criterion fails to capture outliers in certain samples (possibly due to the material information of those outliers), we explore changes to the criterion, e.g. making the interval greater (checking frequencies ranging from 1458 to 1478) and checking for frequencies which are below 20000 within the interval the criterion concerns. The results vary greatly from the original criterion. Though some of the spectra originally ignored by the criterion now become visible, not all regions are sufficiently captured. This indicates the necessity to use other parts of the spectra which appear to be relevant for outliers. The spectra are too big for further manual inspection, which greatly motivates the application of machine learning methods. The frequency criterion will, however, serve as a ground truth in this analysis. Going forward in this section, we aim to evaluate all the following methods by comparing them to the results of the frequency criterion. Examples which best reflect the method's performance in outlier detection will be displayed for comparison with this criterion. This way, we have some knowledge about where outliers are detected. While the criterion is insufficient in detecting all outliers (as demonstrated in this subsection), the general patterns discovered here must be present in the results yielded by the other methods. If the method under analysis fails to produce results corresponding to the frequency criterion, we opt to disregard that method. The desired method optimally produces similar results as the frequency criterion and finds more areas on the samples where we know outliers are present. Ideally, the methods also aid in discovering new outliers.

3.3.2 The standard deviation test

We investigate the data using SDT, a test in which the data is centered around the mean and given a standard deviation of one. With this setup, outliers are defined as points which are separated from the mean by three standard deviations or more. We measure the mean and standard deviation on each frequency from the unbalanced training set; we ignore the balancing to avoid changes to the mean and standard deviation which the balancing helps produce. The values are then used to standardize the spectra belonging to each tumor. A spectrum is deemed to be an outlier if the number of frequencies in that spectrum exceeds an arbitrary value. We approximated the value by performing the test once while monitoring the average number of frequencies which lie three or more standard deviations from the mean. In any given sample, each spectrum includes on average 111 frequencies which fail the test. We specify that a spectrum fails the test if more than 111 of its frequencies are three or more standard deviations away from the mean.

Using this test, many small areas are detected in each sample; it suggests there is something present in those places, but they do not possess a clear shape by which we can decide whether to discard them or not. An example of such a sample is shown in Figure 3.5.

(a) The result of SDT for sample HF-448, Several points are labeled as outliers

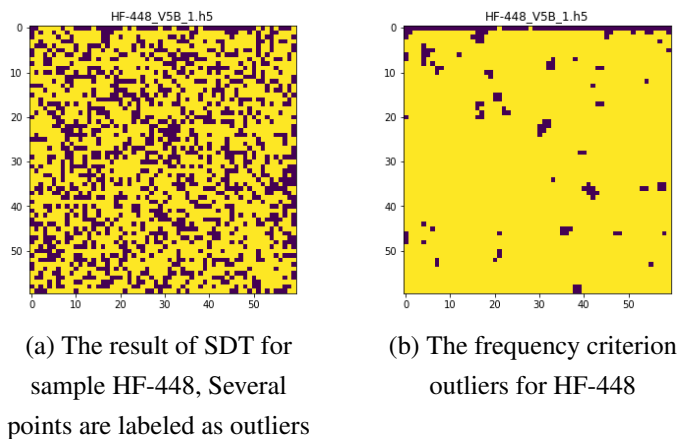(b) The frequency criterion outliers for HF-448

Figure 3.5: A comparison between the SDT and the frequency criterion for sample HF-448.

SDT does not produce results similar to the frequency criterion, some spectra do correspond among the results, but the amount of outliers falsely labeled as outliers by SDT is troublesome. Roughly 50% of the samples in the entire dataset yield similar results with SDT. The method would, as a result of this, discard too much from most samples, depriving the dataset of a great number of tumor spectra. Some areas are formed around the individual spectra, suggesting the presence of an

unknown material, but the sporadic points in the surrounding area make it unclear where that material begins and ends. Furthermore, we must develop a criterion for which points to discard. Such a criterion would need to distinguish between sporadic points which are miss-classified and areas of real outliers. However, within some samples there are areas of outliers correctly labeled, but those areas are not sufficiently defined. One sample with this result is shown in Figure 3.6.
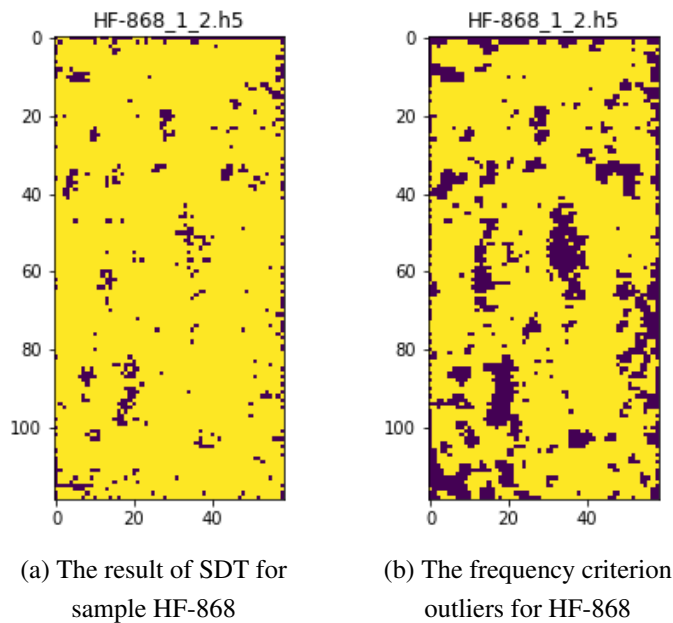

(a) The result of SDT for sample HF-868

(b) The frequency criterion outliers for HF-868

Figure 3.6: A comparison between the SDT and the frequency criterion for sample HF-868. Many spectra correspond to the frequency criterion.

Sample HF-868 is less sporadic compared to HF-448, the outliers are instead formed around common points of interest which strongly suggests outliers are present in that area. The lack of definition in each area however, is not sufficient. The outliers must form concrete shapes with clear definition. The sample suggests outliers are present in the different areas, but all points are not present to make the shapes as defined as they are by the frequency criterion. The sporadic results show that this method is insufficient to detect the majority of outliers in all samples. It must be noted that, despite this underwhelming result, some outliers are detected, suggesting further changes to the method could yield better results, though greedy application is not going to work for all samples. Throughout all the six LGm categories, the method yields the best results for LGm6 where it shares many patterns with the patterns produced by the frequency criterion. Another example of the promise the method has is in sample HF-2852 of LGm3, shown in Figure 3.7.

(a) The result of SDT for sample HF-2852
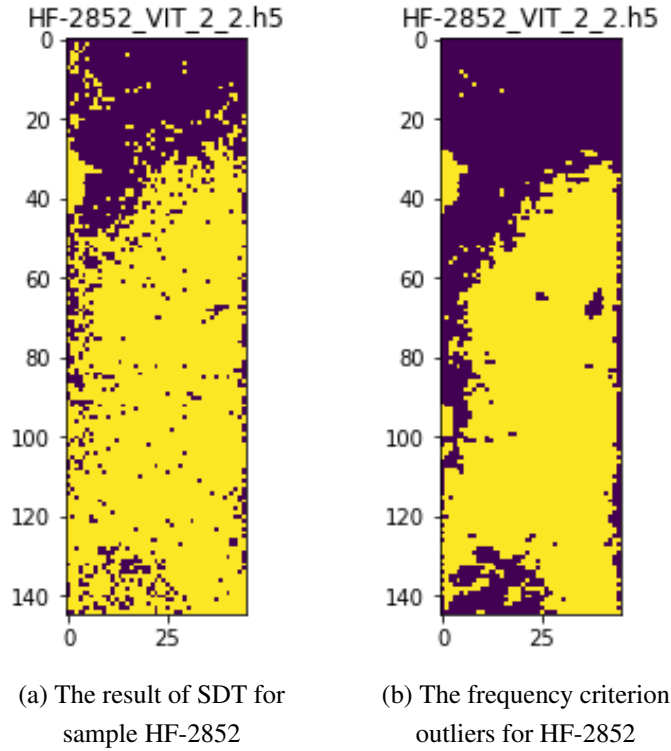
(b) The frequency criterion outliers for HF-2852

Figure 3.7: A comparison between the SDT and the frequency criterion for sample HF-2852.

Sample HF-2852 has a large area in the upper part which consists of necrotic tissue. The spectra of that tissue differs from other spectra sufficiently well, allowing the method to distinguish between tumor and non-tumor with considerable accuracy. This is due to the amount of otherwise healthy tissue present in the sample. The inability of the method to capture all outliers is also apparent despite this, as it allows several smaller spots in the area of the necrotic tissue to be classified as healthy tumor tissue. The area at the bottom of the sample is filled with outliers according to the frequency criterion. These results suggest that the method is best used in detecting necrotic tissue, but not in the context of detecting other kinds of outliers.

3.3.3 The Interquartile range method

Similar to SDT, IRM is a purely statistical analysis method, detecting outliers in terms of which percentile the spectra belong to. The 25th and 75th percentiles are calculated on each frequency for the entire training set. Like SDT, this method yields a varying amount of outliers for each sample. We instead define the allowed number of outlier frequencies within one spectra to be equal to the average number of outlier frequencies within the analyzed sample. Many regions are better repre-

sented by IRM, showing well defined areas where outliers are clearly present. The amount of individual spots are less frequent which shows promise in the method, as e.g. blood is expected to cover a larger area if present. The improvement from the standard deviation test is seen in Figure 3.8.
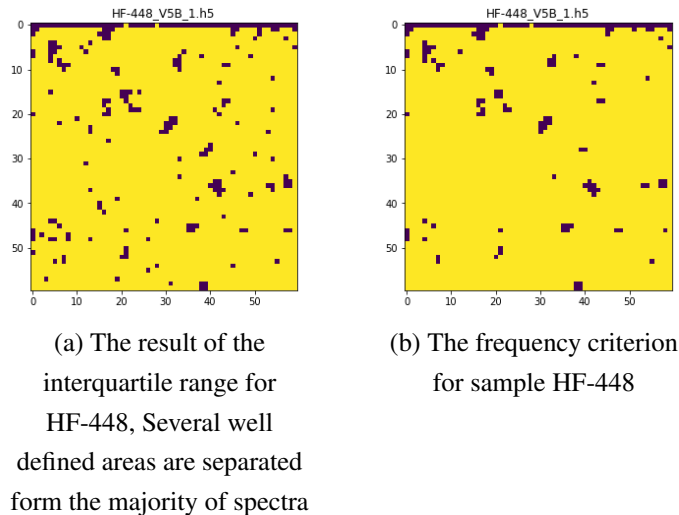

(a) The result of the interquartile range for HF-448, Several well defined areas are separated form the majority of spectra

(b) The frequency criterion for sample HF-448

Figure 3.8: A comparison between IRM and the frequency criterion for sample HF-448.

SDT failed to separate outliers adequately in sample HF-448 while IRM is better suited to detect the outliers in this sample. The upper part of the sample has a well defined line where the sample is presumably cut, meaning the plastic underneath the tissue might be visible. We also note that many outliers detected by IRM also appear to be captured by SDT. While the areas are hard to distinguish among all sporadic spots, the larger spots in Figure 3.8 (a) seem to have some trace in Figure 3.5. The correspondence with the frequency criterion in Figure 3.8 (b) further shows the methods capability in contrast to SDT as the method seems to possess greater ability in defining the areas where outliers are present. There are still some spots appearing randomly around the sample surface which would ideally be ignored, but while we have some confirmation on where outliers are present in certain samples, we do not know exactly where the outliers are. The individual points being labeled as outliers suggests the method struggles with the same issue SDT suffers from. Though it appears to be less severe in all samples belonging to LGm1, there are still a considerable number of spots through all samples within the category. Especially LGm4 have samples for which both methods perform poorly, with a considerable amount of sporadic spots appearing in some samples when applying IRM and a significant lack of spots when applying SDT i.e. None of the methods works sufficiently well to detect the outliers. It should be noted that both methods detect outliers in areas

which the frequency criterion also produces. But the areas are not corresponding well in either method. This issue is apparent in sample HF-2802 of LGm4, shown in Figure 3.9.
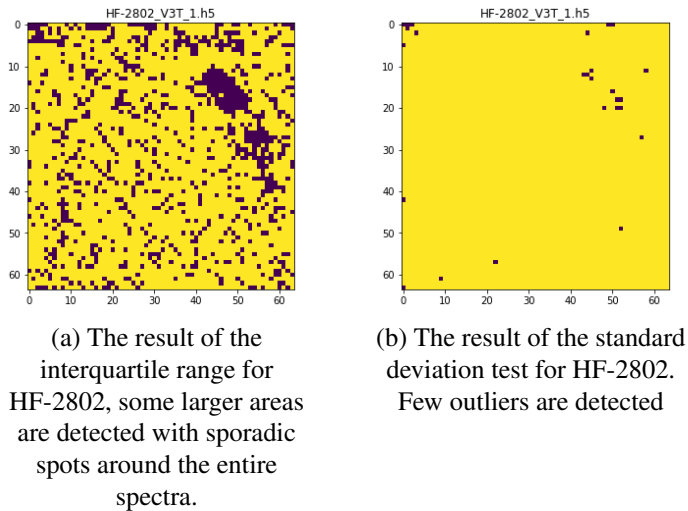

(a) The result of the interquartile range for HF-2802, some larger areas are detected with sporadic spots around the entire spectra.

(b) The result of the standard deviation test for HF-2802. Few outliers are detected

Figure 3.9: A comparison between the interquartile range and the standard deviation test for sample HF-2802. In comparison, the interquartile range locates better defined areas than the standard deviation test, but many sporadic spots are present.

In Figure 3.9, the results of IRM and SDT are compared on sample HF-2802. Both methods yield poor separation between the outliers and tumor spectra. IRM is capable of detecting a large mass of some material on the sample, however, many sporadic spots appear around it, the majority of these spots are tumor spectra which would be discarded by the method. In stark contrast, SDT struggles to detect anything in the sample, only yielding small spots in the larger areas found with IRM. Fewer samples suffer from the stochastic results present in SDT, however all samples are not strictly improvements from SDT. One such example is sample HF-1010 belonging to LGm2, shown in Figure 3.10.

The comparison in Figure 3.10 shows one of few samples where IRM fails to sufficiently separate outliers from tumor spectra. A considerable number of spectra are falsely labeled as outliers, and those spectra seem to form many smaller areas without sporadic points in the surrounding area. In this rare case, SDT exhibits sufficient separation of the outliers, as the detected areas correspond well with the position of known outliers found by the frequency criterion.

Few samples follow the same conclusion however, these varying results show clear signs that neither of the methods are suitable to perfectly rid each sample of outliers. We therefore dismiss them from the analysis, while keeping the results for comparison with the other methods. We continue the analysis by analyzing unsupervised machine learning methods for outlier detection.
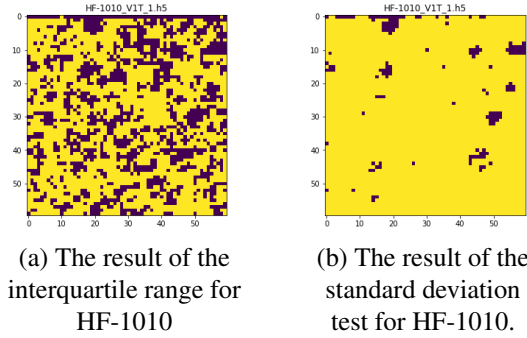
(a) The result of the interquartile range for HF-1010

(b) The result of the standard deviation test for HF-1010.

Figure 3.10: A comparison between the interquartile range and the standard deviation test for sample HF-1010, LGm2.

3.3.4 Hierarchical clustering

The next method for outlier detection is hierarchical clustering, we choose to utilize the agglomerative version of the algorithm. Due to the algorithm's demanding time complexity and memory constraints, we analyze each sample separately to avoid memory errors. Each sample must be given one unique model which then divides the data into the number of clusters specified. This means there will not be a universal model designed to separate all samples. We investigate the results of different distance metrics and choose the *Euclidean distance* as distance metric to measure distance among the clusters. This conclusion is due to the uncertainty in vector shape and angles on which Cosine similarity is dependent. The *Manhattan distance* would be a better choice compared to *Cosine similarity*; however, *Euclidean distance* magnifies long distances, which should aid the algorithm in selecting clusters for agglomerative merging. Next we examine the linkage criteria available. In each case, the algorithm is set to run multiple tests where it separates the data into different amounts of clusters. We choose to initialize six different models to compute between two and seven clusters respectively. Due to the deterministic nature of the algorithm, the results in one cluster will be present in the other clusters as the number of clusters increases.

Single linkage merges clusters which possess points with minimal distance. Should the spectra within the samples be significantly "far apart" in the data, the criterion might start producing many unique clusters in a "chain". If the number of clusters are sufficiently small, the number of cluster separations will be few, and few spectra will be allocated to those clusters. This can result in few separations for some samples, which will render the method unusable for our purposes.

The criterion yields clusters which appear as individual points in the images and fails to detect areas where known outliers are present in the samples, suggesting the aforementioned flaw is present in this methodology. This is apparent as we see few

cluster areas form in any of the initialized models, even if we allow the method to use more than two clusters. All different cluster models fail to separate the outliers and instead separate a small number of points. An example of this phenomenon is displayed in Figure B.6.
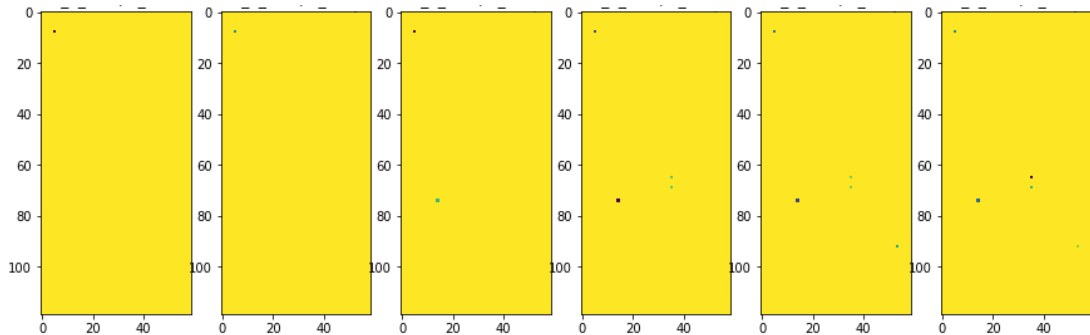

Figure 3.11: Single linkage on sample HF-868 from LGm1: The test fails to detect any outlier areas. Leftmost image is the result of the model computing two clusters. The number of clusters increase towards the rightmost image.

The models fail to detect any areas where outliers are present, only yielding an insignificant number of outliers in the entire sample. Models computing more clusters also fail to find significant areas and smaller spots appear as the number of clusters increase. As the number of clusters increases, several of the outliers seem to belong to their own clusters, which is a sign of the clusters being computed in a "chain" as previously stated. Due to this unsatisfactory result, single linkage will not be used as linkage criterion in this project.

Average linkage yields superior results compared to single linkage since some areas become more defined as we increase the number of clusters. However, the criterion does not have a set number of clusters which is guaranteed to include all outliers for all samples. For certain samples the outliers are visible when forcing the algorithm to agglomerate to two clusters and others only show them once five or more clusters are allowed. It is possible to use the criterion for discarding the outliers if the majority cluster is preserved when computing seven clusters, while the rest of the spectra are discarded. However, this would not remove all outliers and some problematic samples in LGm3 would have the majority of outliers preserved. The improvement from single linkage is made apparent in Figure 3.12.
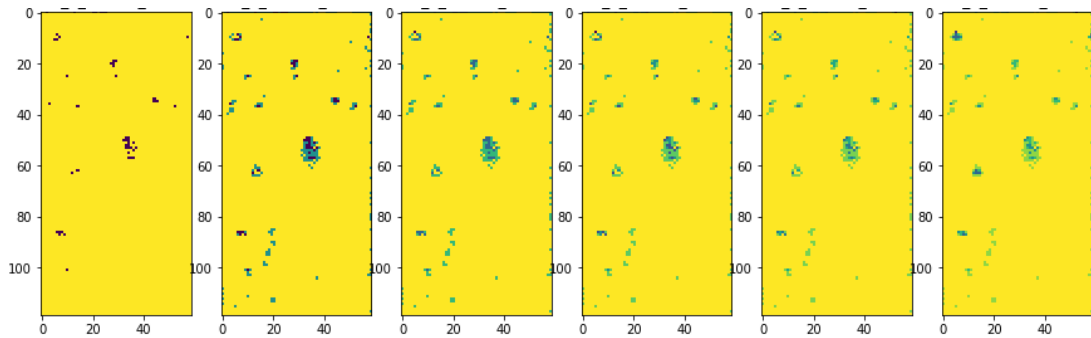
Figure 3.12: Average linkage on sample HF-868 from LGm1: Leftmost image is the result of the model computing two clusters. The number of clusters increase towards the rightmost image.

The model computing two clusters is capable of producing separations where the outliers are present, though it still misses the bigger areas. As the number of clusters increases, the areas become more defined and capture more of the outliers. Despite this, not all outliers are detected despite computing seven clusters. One area should be captured in the lower left corner of the sample. However, only smaller clusters form around that area. Capturing it sufficiently would mean adding more clusters, but the number of clusters which best capture the outliers for all samples is variable in this case. It is a clear improvement over single linkage, but the criterion is still insufficient.

Complete linkage merges the clusters which possess elements with the smallest possible maximal distance between them. The method produces similar results as average linkage, few areas with outliers are detected when fewer clusters are permitted. However, some outliers are present when computing two or three clusters. Computing seven clusters allows the algorithm to detect outliers which are also detected by the frequency criterion. Though these results are not strictly improvements from average linkage, the criterion does manage to detect certain spots of outliers with fewer clusters than average linkage in certain samples. The result of complete linkage on sample HF-868 is seen in Figure 3.13.
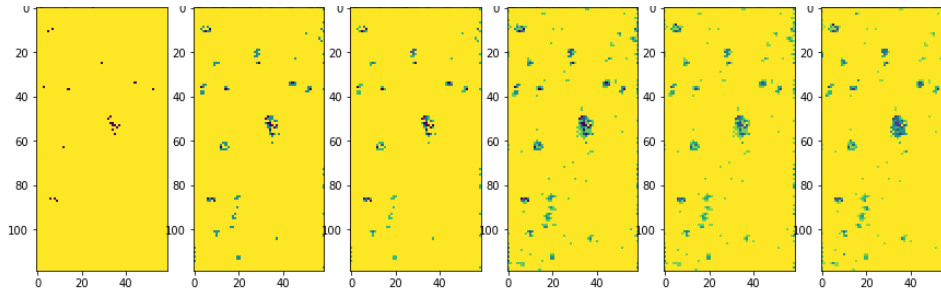
Figure 3.13: Complete linkage on sample HF-868 from LGm1. Leftmost image is the result of the model computing 2 clusters. The number of clusters increase towards the rightmost image.

As is evident in Figure 3.13, much like average linkage, complete linkage produces clearer areas as more clusters are computed. In HF-868, outliers are not detected earlier than average linkage, in fact, the outliers require more clusters to become apparent. A good approximation for the majority of samples appears to be the models computing seven clusters, if a few outliers are allowed to be included in the training phase of the model. The criterion's tendency to produce clusters earlier than average linkage is better displayed in Appendix B. Most samples display similar results; more outliers are detected overall with complete linkage in models computing two or three clusters than models using average linkage. Despite this, all five models fail to detect the outliers found by the frequency criterion. We therefore decide to disregard complete linkage for this project as well.

Ward linkage merges clusters which possess minimal variance between their respective elements and, as such, works well with *Euclidean distance*. We do stress that the clusters are merged by measuring variance among cluster elements and there is no guarantee the outlier spectra should share in characteristics which would result in low inter-cluster variance. Despite this lack of guarantee, the clusters form at the precise location of outliers detected by the frequency criterion. Allowing seven clusters produce a near picture perfect image of the biological tissue from which the spectra were measured. These results show that the algorithm is capable of organizing the spectra according to their visual information, which aids us in understanding the shape and state of the samples. The criterion works considerably well for outlier detection when compared to the other criteria analyzed thus far. It appears to be capable of detecting well defined outlier areas Moreover, the individual points which appear around those areas appear to form smaller groups; these could very well be individual droplets of the same outlier material detected in the larger areas. The promising performance of ward linkage is well represented in Figure 3.14.
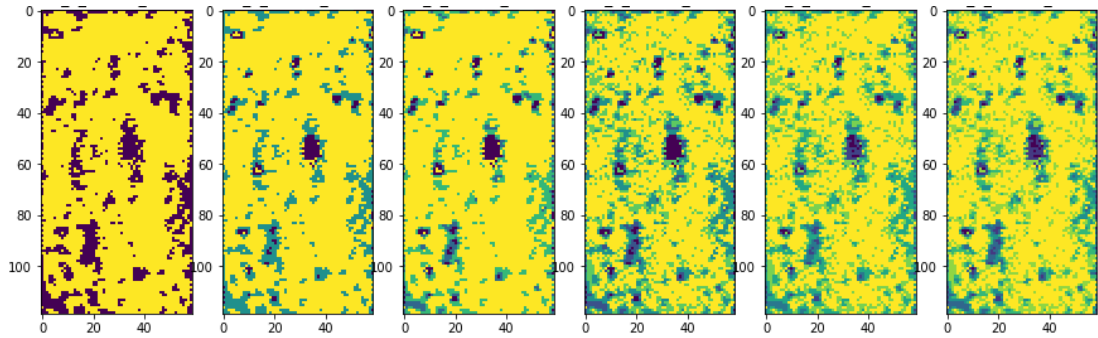
Figure 3.14: Ward linkage on sample HF-868 from LGm1: The leftmost image is the result of the model computing 2 clusters. The number of clusters increase towards the rightmost image.

The outliers identified correspond well with the frequency criterion, and as the number of clusters increase, the surface of the tissue starts to become visible by the different clusters. The model computing two clusters have near perfect resemblance with the frequency criterion. The models computing three and four clusters appear to perform subdivisions of the outlier cluster found in the model computing two clusters. This results tells us that the outliers appear to have significant differences from tumor spectra, which is a great result. We should expect similar results in samples which contain a great number of outliers. Once five clusters are allowed, spectra from healthy tissue starts to become apparent. These results appear to occur in the majority of samples.

The issue is finding a uniform criterion on which we can discard the outliers. We seek to define that criterion in terms of which clusters to discard from the samples following their analysis. Removing every cluster except for the majority cluster in the case where seven clusters have been formed would remove legitimate spectra which are suitable for training a model from all samples. In fact, there is no optimal choice in this case, as certain samples have their outliers sufficiently captured in a setup allowing for two clusters, while others show their outliers in arbitrary numbers of clusters. Furthermore, selecting clusters which contain close to 50% of the spectra would be undesirable in context of maintaining a sizable dataset. By visual inspection, we deem the optimal number of clusters to be three, since many outliers are present in this choice, though the problem is not completely remedied. In some samples, ward linkage separates areas not outlined by the frequency criterion when two clusters are computed. The outliers are instead detected when computing more clusters. This complicates the process of finding a uniform criterion, but the number of outliers which are missed by our current paradigm is considerably small. In particular, sample HF-2485 suffers from this problem; the cluster results are shown
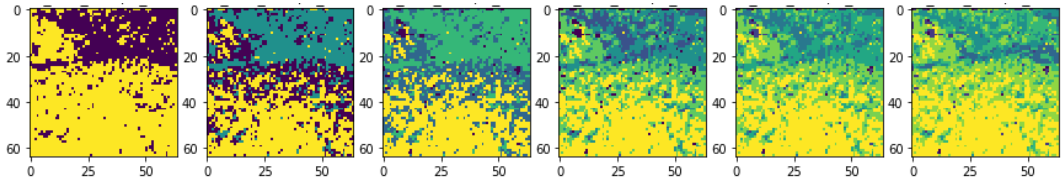
in Figure 3.15.

Figure 3.15: Sample HF-2485 from LGm5, clustered by Hierarchical clustering using ward linkage. From left to right, is shown the results of computing from 2 to 7 clusters respectively. The oultliers are present from image 4 and up.

The models computing two and three clusters actively avoid the concrete spots where the outliers are positioned. In the model computing four clusters, the outliers are detected as dark spots labeled as tumor spectra by the earlier models. The dark spots perfectly correlate with the position of outliers outlined by the frequency criterion. In the model computing seven clusters, the surface of the tissue starts to be replicated. Here, the outliers are displayed in stark contrast to the rest of the tumor material. In this case, we opt to continue with our paradigm of keeping the majority when computing four clusters. This will remove too much in a few samples, but will suffice should no other method yield better results. The alternative would be to use three clusters to preserve the otherwise healthy spectra, but in the interest of training on data devoid of outliers, we opt for four clusters.

3.3.5 K-means clustering

We continue this analysis by performing K-means clustering to detect the outliers. We flatten the training set and reorganize it in random order to avoid bias towards recurrent LGm categories in the dataset. The examples are then used to fit six K-means models to compute two to seven clusters respectively as done with hierarchical clustering. This method has the advantage of being trained on the entire training set whereas hierarchical clustering possesses too great a time and space complexity which makes similar experiments impossible with our current hardware. Under this structure we may now compare the results between sample custers. We observe that the stochastic nature of the algorithm produces results of varying quality. In contrast to hierarchical clustering, K-means does not produce clusters as subdivisions of previously seen clusters. This is due to the algorithm being computed several times with random initialization settings. The final result which the algorithm yields is the cluster state possessing minimal inertia compared to the other computations.

Contrary to all other methods of analysis, this method is able to capture small segments of the upper part of the sample HF-1293, shown in Appendix B. While

the comparison of the same sample among the different models lacks consistency in this setting, the comparison between the model results among the different samples are promising. We find that the model in which two clusters are computed, the samples are divided in ways which correspond with the frequency criterion. Moreover, in samples where minimal amounts outliers are present, the clusters seem to form around healthy tissue, which in turn creates an image resembling the surface of the sample-tissue. In certain cases the clusters fail to capture known outliers but other models allowing for more clusters capture them sufficiently well. One example of this is sample HF-868 where the two cluster model fails to detect the relevant outliers but the model computing three clusters capture the outliers in near perfect resemblance to the frequency criterion. The clusters computed by the different models are displayed in Figure 3.16.
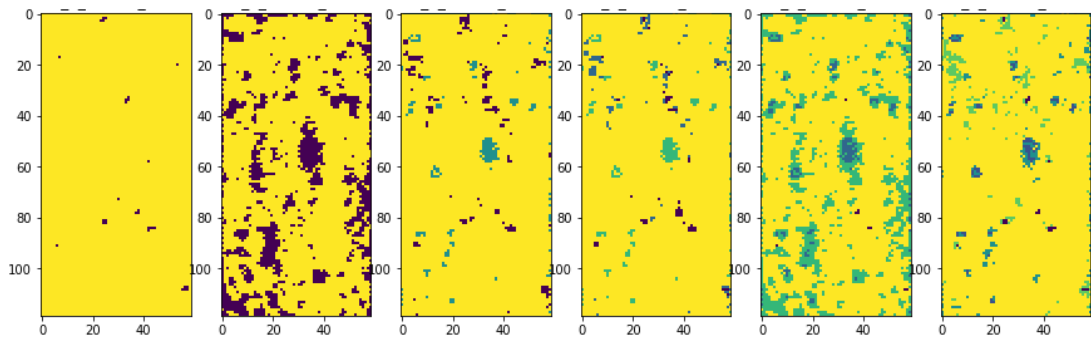

Figure 3.16: K-means clustering on sample HF-868 from LGm1: Leftmost image is the result of the model computing 2 clusters. The number of clusters increase towards the rightmost image.

The other models lose some of the outliers around the shapes present while still capturing the center of the shapes. The results of the frequency criterion returns in the model computing six clusters, but this is again lost in the model computing seven clusters. Like ward linkage for hierarchical clustering, there are some samples where the majority cluster is hard to evaluate; one such sample is HF-2544 which shifts the majority cluster between the model computing two clusters and the rest of the models. Due to the variety among the different models, finding a uniform criterion for detecting outliers is problematic. Many samples are such that the models steadily increase the number of outliers clustered, but this relationship is not constant through all samples, making it insufficient for use as criterion. The shifting of the majority cluster in the aforementioned sample further complicates matters, since the majority cluster may not be capturing healthy tissue in some samples. For this reason, we deem the method insufficient for separating outliers, though we note the promise in capturing information about the visual aspects of the sample-tissues,

which makes the method comparable to ward linkage for hierarchical clustering.

3.4 Post analytical feature extraction

Concluding this chapter, we select the method of analysis best suited for separating outliers from the spectra and extract the features which best separate the data into the different LGm categories. The feature extraction is done by using the training set exclusively. Based on the analysis performed in this chapter we choose to apply hierarchical clustering using ward linkage as linkage criterion. The samples within the training set are first rid of the outliers detected by performing the chosen clustering method. The model computes three distinct clusters of spectra for each sample separately and retains the cluster which contains the most spectra i.e. the spectra corresponding to the yellow colors in the figures shown in this chapter. We then repeat the procedure for feature extraction as done in the beginning of this chapter. We balance the training data, since the category distribution has changed due to removing spectra from each category. Feature selection is done with the f-classif method to score each frequency according to the ANOVA F-values. The 70 frequencies possessing the greatest scores after the method's application are then extracted. The index of the 70 most descriptive features of the training set are shown in Appendix A. In the set of features extracted from the curated data, twelve features are shared with the features drawn from the initial balanced training set. Of these intersecting features, none are the features which the frequency criterion concerns. This indicates that the outliers originally affected the Anova F-values computed by f-classif. The intersection of the features also show certain frequencies were correctly extracted from the non-curated training set. The features extracted from the curated training set are also positioned on different regions on the spectrum. The newer features show interest in frequencies starting early in the spectrum. More than half of the frequencies of interest are also positioned on the right end of the spectra, suggesting considerable amounts of information are located there. In case it becomes necessary to reduce the size of the data, these are the features we recommend be used instead. The spread across the entire spectrum suggests these features are descriptive enough to help machine learning models learn the sample-to-LGm relationship sufficiently well. In case the models struggle with training on these features exclusively, the algorithm may be easily adjusted to extract more features. We expect that 70 features should be enough for learning relationships within this data, especially since almost all features lie in close proximity to other features i.e. the relevant frequencies appear to be grouped with other nearby frequencies. The most irregular features in this regard are the frequencies: 23 and 722. The fact these

frequencies appear with no "neighbour" frequencies suggests the data would require more features to adequately be represented in this simplified form.

Chapter 4

Applying the Data

Following the curation of the data in the previous chapter, the number of spectra available in each data set decrease by approximately 25%. The distribution of the data remains the same, as the amount of spectra within each category retain the relative sizes to the other categories. In this chapter we present the proposed pre-processing methods for the data. We evaluate the data curation and pre-processing techniques by initializing a deep learning model and training it to predict the desired category of each sample. The results are then presented and analyzed.

We proceed to make the data suitable for application with machine learning methodology. The first method of pre-processing is baseline correction. The baseline of a spectrum is the minimum value each wavelength frequency has. The extraction of the spectral signal from the spectrometer may, depending on the settings of the instrument, produce different minimal values for each frequency. This may lead to smaller spikes appearing in otherwise "flat" areas of the spectrum. Baseline correction alleviates these issues by removing the excess baseline in all frequencies of the spectra, which simplifies analysis among the different frequencies. In context of the Raman spectra available in this project, the baseline by which the spectra are skewed is non-linear, and appears to have a polynomial baseline. This is apparent from the wave-like shape of all spectra, where frequencies are minimal relative to the rest of the frequencies which portray spikes in the spectral wave. In turn, some methods require a polynomial grade which is an approximation of the polynomial wave the baseline appears to originate from. This approximation of the polynomial grade may present issues, as it appears to require analysis of each spectrum in separation from the others. Nor is there any indication that the polynomial grade is uniform across all spectra in the data set. To avoid approximation of the polynomial grade we utilize the ZhangFit-method, which has support for Python through the BaselineRemoval library. The method utilizes the adaptive iteratively reweighted penalized least squares (airPLS) algorithm which iteratively approximates the base-

line of the spectrum given without additional information regarding the structure of the spectrum [51]. For some spectra within the data set, the algorithm reaches the maximal amount of allowed iterations before the spectra are returned, This occurs in approximately 1000 spectra. However, this setback is ignored, as it is less than one percent of the training spectra.

Machine learning methods are susceptible to spectra which have large variance among values. Frequencies inside the individual spectra vary tremendously, as spikes within each spectrum may differ from the baseline by a value of $10,000$ and more in many cases. It is clear that some method of normalization is needed to make the spectra applicable with machine learning methods. We opt to use z-score standardization and apply it to the frequencies within the training set. Standardization is performed as follows: Compute the mean and standard deviation of all frequencies through the whole training set. This results in two lists of length 1738 where the indices of those lists correspond to the mean and standard deviation of the respective frequencies. Each value of the spectra is then standardized by applying z-score standardization to each frequency by using the corresponding mean and standard deviation from the initialized lists. This method is preferred as it brings smaller values close to zero on each frequency while maintaining the larger values for the bigger spikes on the spectra within the training set. The features are however not sufficiently scaled down as many frequencies still exceed a value of 60 in some spectra.

In further attempts to scale the data into a range which works better for machine learning methods, we also apply normalization by the maximum absolute value. Following standardization, the maximum absolute value of each frequency is measured and stored in a list. The data set is then normalized by dividing each value in each frequency by the corresponding maximum absolute value stored. This retains the sparsity of the data while scaling all values down to a range between negative one and one.

We also define an augmentation method to better regularize the learning process. We train the model by selecting an equal amount of random spectra from each category for every batch used for training, this is done on the training set. Every batch will be balanced as a result, which avoids the problem of unbalanced data sets. The batch is then augmented before the batch is passed to the pre-processor. Augmentation is performed by adding a skewed line to the batch of data which introduces a random, linear baseline to each spectrum in the batch. Each frequency in each spectra in the batch is then given additive, normally distributed noise which is drawn from 1738 normal distributions, each generated from the means and standard deviations extracted from the data in the pre-processing step. This ensures the noise

is within range of the usual values present for the respective frequency. To allow the model a chance to learn the real data patterns, data augmentation is skipped randomly with 30% probability. The augmentation and pre-processing pipelines are displayed in Appendix D

We create a deep convolutional neural network model and train it using the training set. The model architecture is based on the architecture presented by Liu et al. [15] and is five layers deep, consisting of two convolutional layers and three dense layers (one of which is the output layer). The input is always a one-dimensional vector consisting of 1738 elements (one neuron for each spectral frequency). The one-dimensional convolutional layers consist of 16 and 32 kernels respectively; both layers use the leakyReLU activation function and the kernel sizes are 21 and 16 respectively. Both layers use batch normalization and max pooling with a size of two. The model then flattens the result from the latter convolutional layer to allow for dense layers. Following the flattening layer, a dropout is provided with a dropout of 20%. The two dense layers before the output layer are sized 128 and 32 respectively and both use the tanh activation function. Both layers use batch normalization and the latter layer is followed by a dropout of 40% followed by Gaussian noise generated from a normal distribution with a mean of zero and a standard deviation of 0.15. The output consists of six neurons and uses the softmax activation function to form a probability distribution of the input signal. The loss is then calculated using categorical cross-entropy which is optimized using the Adam optimizer with a learning rate of 0.003. All layer weights are initialized randomly from a normal distribution with a mean of zero and a standard deviation of 0.1. After compilation, the model consists of $1,742,374$ total parameters, of which 416 are non-trainable. A figure displaying the architecture is shown in Appendix E.

Several trials on the data suggest that the size of this architecture is arbitrary and provide little in terms of performance regarding the predictions of the model. We also create variations of the architecture, some of these variations are made with one type of activation function (the activation functions we test are tanh, LeakyReLU, ReLU and sigmoid). Changes to the convolutional layers are also arbitrary; strides and pooling sizes larger than two have been tested. The change to the convolutional layers drastically decreases the amount of learnable parameters in the model which makes the model faster to train. Before the model is initialized we set the random seed in numpy, os.environ and tensorflow to 6 (a value chosen arbitrarily). The resetting of the seeds is important, as it makes the random initializations predictable and, as a consequence, reproducible. The model is trained on balanced batches which consists of 600 spectra (100 spectra per unique category). The batch is generated and augmented before being pre-processed and given to the model where it is

then trained on for a duration of two epochs, the entire model trained in this fashion for 40 epochs.

The first test we perform is to deduce whether the data can be learned by the model or not. We perform this test by separating the training set into two smaller distinct sets. Before separation, the entire set is sorted into a random order which scatters the spectra within randomly; the model is then trained on the first set and evaluated on the other. In this setting, the model manages to learn and generalize well to both halves of the training data. We manage to get these results by using the current pre-processing method discussed earlier in this chapter. Omitting the maximum absolute value normalization method when training in this setting prolongs training drastically and prevents model generalization for the unseen part of the training set. While the accuracy for all spectra is insufficiently low (approximately 82% after training), letting the model train for longer periods of time appear to lead to better results. The overwhelming majority of correct predictions suggest the model is well suited for predicting the categories given all spectra from a sample. More spectra given to the model increases the probability of correctness in the prediction. The model even performs well on unseen spectra (drawn from the same sample used for training) suggesting homogeneity among spectra originating from the same sample. However this does not hold true for the validation data consisting of entire unseen samples. The predictions for the spectra within the validation data are sporadically scattered across many classes. LGm2 is severely underrepresented in the predictions generated by the model and few predictions appear correct through the majority of categories. LGm1 is the only category which is correctly predicted by the model. All other categories fail to be accurately represented, even the majority predictions fail as the majority of predictions are focused on other categories. The confusion matrices of the predictions for the training set and validation set are displayed in Appendix C. In hope of alleviating this issue, we rejoin the split training set into one complete data set and resolve to training on the entire training set while using the validation set for validating the performance of the model.

The model is fully capable of generalizing to the training set which is consistent with the previous result. The number of epochs must be increased further for the model to adequately learn the training data. We therefore increase the number of epochs from 40 to 80 which allows the model accuracy to reach over 90% accuracy on the training data. However, the accuracy is not reflected in the validation data. As in the setting with the split training data, the model achieves approximately 30% accuracy on the validation data. This result is constant through multiple runs in which we change the model in various ways, i.e., change of activation functions, layer sizes and amounts and regularization layers such as dropout and Gaussian

noise. By examining the confusion matrix made out of the predicted values and expected values we discover that the model tends to produce predictions mainly for categories LGm1, LGm4, LGm5 and LGm6. The model is seldom able to perform satisfactory predictions for more than two categories. The categories the model predicts seem to be a result of the order in which the model encounters spectra from the training set (which is dependent on the mini-batch parameter given to the model when training starts). The fact that the model can generalize to unseen training data but not to the pre-processed validation data suggests that the spectra are heterogeneous among the samples which makes it hard to generalize to all categories. How to alleviate this issue and other possible sources this problem stems from is a speculative matter and elaborated upon in the next chapter.

Chapter 5

Conclusion

In this chapter we present conclusions regarding the analysis of spectra for detecting outliers, the performance of the machine learning model presented in Chapter 4 and provide suggestions for further analysis of the tumors and feature selection.

The features extracted from the data utilize the ANOVA F-value to score the features in the data. These features are extracted from the training set on principle, as we want to avoid any bias towards the validation and test sets. The features presented in Appendix A are the features extracted before and after the samples have been separated from the outliers. Furthermore, we have found that the extracted features vary greatly depending on which samples are present in the training set, which brings the consistency of the results into question. This is perhaps not surprising given the reliance of variance in ANOVA. Switching even one sample in the training set has the potential to shift the mean of the entire set. Furthermore, all spectra have more than 1700 frequencies used in the calculations, which may very well cause the squared distances to change considerably. Yielding a different F-value for each frequency. The use of f-classif is due to its capability of handling the negative values present within the data. There are other methods better suited for feature selection in the context of classification e.g. chi-squared which does not handle negative values. For future tests, we would examine a method for transforming the data, such that all frequencies have a positive scope, which would allow feature extraction using chi-squared as a scoring function for SelectKBest.

The modeling results suggest that heterogeneity keeps the model from generalizing to unseen data. Through multiple tests, where the architecture of the model has been modified in various ways, we conclude that the architecture appears arbitrary for training processes that last for approximately five hours. Provided the pre-processing methods mentioned in Chapter 4 are used, the model always manages to learn the training set with accuracy ranging from 90% and above. The model's performance on the validation set is always insufficient due to the model

over-representing certain categories. We also replaced all the samples in the validation set with samples drawn from the training set to test if any samples within the original validation set remain problematic after the outlier removal procedure. However, the results remain the same after training; this suggests the problem lies in heterogeneity among spectra from different samples rather than problematic samples in the validation set. The improvements to the model's performance appear to stagnate after 100 epochs, but it is still uncertain the model cannot improve further with a smaller learning rate, trained on exponentially more epochs. Deep learning models are known to require training for days and even weeks in some cases. We did not explore this possibility and consider it a worthy effort, as the longer training time may result in surprising results. Liu et al. also introduce a custom loss function which takes the distribution of the different categories into account [15]. We have attempted to replicate this loss by introducing weights proportional to the different category distributions, which tune the gradient during training. This, did however not improve performance. There might be an improvement by implementing the custom loss function and we plan to consider it in the future.

We also believe the classes which the model appears to prefer should be examined further; if the problem is independent of the model, the issue is then to be found either in the pre-processing methods or in the analysis stage explained in Chapter 3. We perform baseline correction on the spectra available, but the spectra in the dataset are actually selected frequencies from the complete spectra. It is possible the baseline correction algorithm is unable to remove the baseline sufficiently when all spectral signals are unavailable. Baseline correction might therefore not be suitable for this data and should be reconsidered during the analysis stage. Alternatively, different methods for baseline correction may be tested on the data. One possible alternative method would be to approximate the baseline using linear regression. Standardization retains huge values in certain frequencies; it is possible that frequencies which possess large values are outliers (provided the frequencies are drawn from a normal distribution) and should therefore be removed. Maximum absolute value normalization is something we are certain is required for the model to comprehend the data, due to the drastic change in scope for the values within the spectra.

The analysis in Chapter 3 shows that ward linkage is sufficient in detecting outliers compared to the frequency criterion. However, the outliers detected for certain samples appear after several other areas have been separated into other clusters. One interpretation of this is that the initial clusters differ more from the majority compared to the outliers and are therefore outliers themselves. We use this interpretation in this thesis, but there is another interpretation based on the definition of

ward linkage. Ward linkage depends on the definition of variance, which depends on the mean of the sample under analysis. It is possible that certain clusters of tumor spectra may form prematurely due to having an inter cluster mean which differs considerably from the rest. In cases where few outliers are present in the sample, this may cause outliers to appear after the appearance of other clusters. This is shown in sample HF-2485, where clusters avoid the known outliers and instead detects the outliers once four clusters are allowed. This case requires a different solution regarding which cluster should be removed from the sample. The suggestion we give as an alternative solution is to use the distance between the means of the different clusters. The mean of the outlier cluster should be sufficiently distant from other clusters to be used as a discriminator. This would need further testing for confirmation. Moreover, clustering methods are only usable in cases where outliers are known to be present; using clustering on a sample devoid of outliers will still produce clusters around parts of the sample, which is shown in the figures of Chapter 3. Allowing more clusters than necessary for outlier detection causes clusters to form around other tumor spectra which are usable in the training set. We also attempted to use baseline correction on the spectra before the clustering analysis, but this does not yield similar results, outliers become harder to spot and clusters appear to miss major areas where outliers are possible. The same occurs when using the features extracted by f-classif. In earlier tests, we have tried to separate the spectra by the frequency criterion, labeling all spectra as either outlier or non-outlier. Using f-classif, we have extracted the features which best separate the data into outliers and non-outliers and attempted clustering following feature extraction. The results are mixed, as the strategy made the model separate outliers extremely poorly compared to the strategy where all features were used. Thus, we conclude that raw spectra are optimal for outlier detection using hierarchical clustering with ward linkage, utilizing the Euclidean distance metric.

These suggestions may yield better results for the model. Our tests suggest heterogeneity is the key problem in this analysis. However, it is not certain that this is the correct conclusion. It is still unclear how the heterogeneity among tumor samples is preserved in the Raman spectra we have available. One possible issue for this project is that the number of tumor samples available from unique patients is lower than 50. It is possible the model requires more unique patient samples to adequately learn the characteristics of the different categories. DL models are extremely reliant on large sets of data, and it appears the data is the source of our conflicting results, rather than methodology. This problem is unfortunately hard to mitigate, as extracting and scanning new samples require a tremendous amount of manual labor. The dependence on more patients suffering from glioma would also

be a horrible necessity.

Svensk Sammanfattning

Gliom är en typ av cancer som formas i hjärnan från gliacellerna. Tumörer som konsekvent formas av sjukdomens effekt kategoriseras av Världshälsoorganisationen (på engelska "*World Health Organization*") genom olika grader som beskriver hastigheten med vilken cancern sprids, samt dess aggressivitet. Cancerns effekt på gliompatienterna kan variera avsevärt mellan huvudvärk, illamående eller komplikationer gällande hjärnans funktion (t.ex. förvirring, problem med att prata och kommunicera och epileptiska anfall). En patient som diagnostiseras med gliom har ett fåtal år kvar att leva, det är ovanligt att patienter överlever i mera än fem år [2, 3, 4]. Diagnoseringsprocessen inkluderar ett ingrepp, där sampel av tumören extraheras från patienten. Samplen analyseras sedan i labbet för att undersöka tumörens grad och bestämma den optimala medicinska kuren. Denna analys, följande samplets extrahering, kan räcka ett obestämt antal veckor. I denna avhandling beskrivs en analytisk process där vi analyserar Ramanspektra extraherat från gliomtumörer, tagna från 45 patienter. Från vissa patienter har flera sampel av samma tumör tagits, vilket ger ett större antal sampel än patienter. Analysens syfte är att förbereda alla spektra för användning i maskininlärningsmetoder. Detta innebär att alla sampel måste analyseras för att ta bort de spektra som inte kommer från tumörmaterial. Det är sannolikt att en delmängd av alla spektra från ett givet sampel kan ha kommit från t.ex. blod, plast som reflekteras under tunna bitar av samplet och nekrotiska celler.

Ramanspektroskopi används pga. den information som finns i varje spektra samt dess användning i tidigare projekt med maskininlärning [13, 14]. Ett spektrum består av 1738 olika frekvenser; en del av analysen undersöker vilka av dessa frekvenser som bäst delar in alla spektra i olika kategorier. Kategorierna är baserade på olika sorter av mutationer i IDH-generna. Dessa kategorier har identifierats av Ceccarelli et al. [9] och påstås vara ett bättre sätt att identifiera en bra medicinsk kur, än de grader som för tillfället används. De frekvenser som bäst delar in alla spektra i kategorierna beräknas före och sedan efter att spektra från icke-tumörmaterial har separerats från tumörspektra.

Analys

Analysen börjar med att avlägsna vissa sampel som visar sig vara problematiska att analysera. Två sampel avlägsnas, ett sampel från patient HF-1887 innehåller spektra som ligger på en kurvad grundlinje, vilket innebär att värdet på frekvenserna stiger stegvis från den första frekvensen till den sista. Ett högt värde på en frekvens indikerar information från punkten där spektrumet är taget. Då grundlinjen inte är rak blir det omöjligt att jämföra olika frekvenser i spektrumet. Alla sampel från patient HF-3097 har en konsistent grundlinje med alla andra sampel, men det finns ett betydligt större antal av frekvenser med enorma värden jämfört med andra sampel. Vi väljer att avlägsna alla sampel från patient HF-3097, eftersom den enorma mängden höga frekvenser i alla spektra tyder på att spektrometern har gett felaktiga värden.

Vi fortsätter genom att balansera datamängden enligt kategorierna som vi vill separera alla spektra i. Det finns en stor variation mellan antalet spektra tillhörande varje kategori. Vi delar in alla sampel i olika datamängder som kan ska användas i maskininlärning. Dessa är träningsmängden, valideringsmängden och testmängden. Eftersom det finns en risk för att tumörerna är heterogena, bestämmer vi att dela in dessa mängder enligt sampel, dvs. åtminstone ett unikt sampel från varje kategori finns i varje datamängd. Maskininlärningsmodeller måste kunna lära sig dela in ett spektrum i den kategori spektrumet tillhör genom att träna på träningsmängden. Om detta steg ignoreras och olika spektra från samma sampel används för att träna och validera modellen, kommer resultatet inte vara trovärdigt om alla tumörer är heterogena. Efter mängdseparationerna kan vi balansera träningsmängden genom att beräkna antalet spektra tillhörande varje kategori i mängden. Antalet spektra i träningsmängden tillhörande kategori n kan då beskrivas genom $|LGm_n|$. Varje kategori balanseras genom att kopiera varje spektrum i en kategori x gånger, då x är resultatet av divisionen mellan antalet element i kategorin som utgör majoriteten i mängden och antalet spektra i kategori n. Detta beräknas enligt $x = \lfloor \frac{|LGm_m|}{|LGm_n|} \rfloor$ där $\lfloor$ och $\rfloor$ antyder avrundning nedåt av kvoten. De frekvenser som bäst beskriver samplets kategori beräknas sedan genom användning av *f-classif-metoden* i SKlearn biblioteket i Python [33].

För att identifiera icke-tumörspektra testar vi olika metoder. Dessa metoder är standardavvikelsetestet, kvartilavståndet och oövervakade inlärningsmetoder som *hierkisk klustring* och *K-means-klustring*. Dessa metoder jämförs med frekvenskriteriet, vilket är ett kriterium baserat på frekvenserna 1463 till 1473 på alla spektra. Om någon av dessa frekvenser är under 5000 på ett spektrum, är det spektrumet från ett icke-tumörmaterial. Standardavvikelsetestet och kvartilavståndet ger lik-

nande resultat på majoriteten av sampel. Av dessa två är det kvartilavståndet som ger resultat liknande vad frekvenskriteriet ger. *K-means-klustring* lyckas ge resultat som stämmer med frekvenskriteriet, algoritmen lyckas även hitta andra regioner på samplet som frekvenskriteriet inte hittar. Denna analys utförs genom att initialisera sex modeller som delar in samplet i två, tre, fyra, fem, sex och sju kluster. Mellan alla dessa finns det inte ett klart bästa alternativ för att identifiera icke-tumörspektra i varje sampel. Med *hierarkisk klustrings* undersöker vi olika länkningskriterier som finns implementerade i SKlearn. Dessa är *single-koppling*, *average-koppling*, *complete-koppling* och *ward-koppling*. Av dessa kriterier, är det *ward-koppling* som producerar bäst resultat. Dessa resultat är jämförbara med frekvens kriteriets resultat och de resultat som *K-means-klustring* uppnår. Metoden är också konsistent och kan hitta alla icke-tumörspektra i majoriteten av sampel med tre kluster. I vissa sampel där antalet icke-tumör spektra är oansenligt behövs det fyra kluster eller mera.

Användning av datan

Vi väljer att separera icke-tumörspektra från tumörspektra genom att använda *ward linkage* med *hierarchical clustering* algoritmen. Alla spektra går nu igenom en förberedande process som maskininlärnings modeller kräver. Grundlinjen på alla spektra tas bort genom *ZhangFit* metoden i Python. Alla frekvenser i varje spektra är sedan standardiserade genom att subtrahera varje enskild frekvens med den frekvensens medeltal, differensen divideras sedan med standardavvikelsen för den frekvensen. Alla frekvenser normaliseras sedan genom att dividera varje enskild frekvens i varje spektra med det maximala absolutbelopp för den frekvensen. För att testa datans användbarhet efter den förberedande processen, skapar vi ett djupt neuralt nätverk för att klassificera alla spektra enligt deras respektive kategorier Ceccarelli et al. [9] presenterat. Modellens arkitektur beskrivs och dess prestanda presenteras.

Slutsats

Flera test på olika modellarkitekturer tyder på att arkitektur inte har en betydande inverkan på modellens prestanda, förutsagt att arkitekturen är djup nog. Modellen misslyckas klassificera alla spektra och har en tendens att föredra vissa kategorier över andra. Vi ger förslag för hur de processer vi använt kan förbättras i hopp om att kunna hitta en bättre modell i framtida studier. Dessa förslag är alternativ som inte avsetts under analysens utförande. Exempel på dessa är att använda alternativa metoder för att avlägsna grundlinjen samt förbättring av den analytiska metoden för

att identifiera icke-tumörspektra genom att avsee klustrens avstånd från varandra. En klar förbättring på modellens prestanda är att samla mera sampel från gliompatienter i framtiden, men denna process är inte önskvärd pga. tiden som krävs för att samla dessa sampel samt behovet av lidande patienter.

Bibliography

[1] C. S. von Bartheld, J. Bahney, and S. Herculano-Houzel, "The search for true numbers of neurons and glial cells in the human brain: a review of 150 years of cell counting," *Journal of Comparative Neurology*, vol. 524, no. 18, pp. 3865–3895, 2016.

[2] S. Jäkel and L. Dimou, "Glial cells and their function in the adult brain: a journey through the history of their ablation," *Frontiers in cellular neuroscience*, vol. 11, p. 24, 2017.

[3] O. Gallego, "Nonsurgical treatment of recurrent glioblastoma," *Current oncology*, vol. 22, no. 4, p. e273, 2015.

[4] F. E. Bleeker, R. J. Molenaar, and S. Leenstra, "Recent advances in the molecular understanding of glioblastoma," *Journal of neuro-oncology*, vol. 108, no. 1, pp. 11–27, 2012.

[5] S. L. Maas, E. R. Abels, L. L. Van De Haar, X. Zhang, L. Morsett, S. Sil, J. Guedes, P. Sen, S. Prabhakar, S. E. Hickman, *et al.*, "Glioblastoma hijacks microglial gene expression to support tumor growth," *Journal of neuroinflammation*, vol. 17, pp. 1–18, 2020.

[6] A. Dirkse, A. Golebiewska, T. Buder, P. V. Nazarov, A. Muller, S. Poovathingal, N. H. Brons, S. Leite, N. Sauvageot, D. Sarkisjan, *et al.*, "Stem cell-associated heterogeneity in glioblastoma results from intrinsic tumor plasticity shaped by the microenvironment," *Nature communications*, vol. 10, no. 1, pp. 1–16, 2019.

[7] K. Vigneswaran, S. Neill, and C. G. Hadjipanayis, "Beyond the world health organization grading of infiltrating gliomas: advances in the molecular genetics of glioma classification," *Annals of translational medicine*, vol. 3, no. 7, 2015.

[8] Y. Hirose, H. Sasaki, M. Abe, N. Hattori, K. Adachi, Y. Nishiyama, S. Nagahisa, T. Hayashi, M. Hasegawa, and K. Yoshida, "Subgrouping of gliomas

on the basis of genetic profiles," *Brain tumor pathology*, vol. 30, no. 4, pp. 203–208, 2013.

[9] M. Ceccarelli, F. P. Barthel, T. M. Malta, T. S. Sabedot, S. R. Salama, B. A. Murray, O. Morozova, Y. Newton, A. Radenbaugh, S. M. Pagnotta, *et al.*, "Molecular profiling reveals biologically discrete subsets and pathways of progression in diffuse glioma," *Cell*, vol. 164, no. 3, pp. 550–563, 2016.

[10] L. Dang, K. Yen, and E. Attar, "Idh mutations in cancer and progress toward development of targeted therapeutics," *Annals of Oncology*, vol. 27, no. 4, pp. 599–608, 2016.

[11] D. A. Long, "Raman spectroscopy," *New York*, pp. 1–12, 1977.

[12] P. Graves and D. Gardiner, "Practical raman spectroscopy," *Springer*, 1989.

[13] M. K. Maruthamuthu, A. H. Raffiee, D. M. De Oliveira, A. M. Ardekani, and M. S. Verma, "Raman spectra-based deep learning: A tool to identify microbial contamination," *MicrobiologyOpen*, vol. 9, no. 11, p. e1122, 2020.

[14] C.-S. Ho, N. Jean, C. A. Hogan, L. Blackmon, S. S. Jeffrey, M. Holodniy, N. Banaei, A. A. Saleh, S. Ermon, and J. Dionne, "Rapid identification of pathogenic bacteria using raman spectroscopy and deep learning," *Nature communications*, vol. 10, no. 1, pp. 1–8, 2019.

[15] J. Liu, M. Osadchy, L. Ashton, M. Foster, C. J. Solomon, and S. J. Gibson, "Deep convolutional neural networks for raman spectrum recognition: a unified solution," *Analyst*, vol. 142, no. 21, pp. 4067–4074, 2017.

[16] D. Rowntree, *Statistics without tears: A primer for non-mathematicians.* Scribner Book Company, 1981.

[17] S. So, "Why is the sample variance a biased estimator?," *Griffith University, Tech. Rep.*, vol. 9, 2008.

[18] H. Nobach, "Practical realization of bessel's correction for the bias-free estimation of the auto-covariance and the cross-covariance functions," 2020.

[19] R. C. Geary, "The ratio of the mean deviation to the standard deviation as a test of normality," *Biometrika*, vol. 27, no. 3/4, pp. 310–332, 1935.

[20] H. Vinutha, B. Poornima, and B. Sagar, "Detection of outliers using interquartile range technique from intrusion dataset," in *Information and Decision Sciences*, pp. 511–518, Springer, 2018.

[21] S. Walfish, "A review of statistical outlier methods," *Pharmaceutical technology*, vol. 30, no. 11, p. 82, 2006.

[22] Y. Dovoedo and S. Chakraborti, "Boxplot-based outlier detection for the location-scale family," *Communications in statistics-simulation and computation*, vol. 44, no. 6, pp. 1492–1513, 2015.

[23] H. Scheffe, *The analysis of variance*, vol. 72. John Wiley & Sons, 1999.

[24] R. Lowry, "Concepts and applications of inferential statistics," 2014.

[25] N. Sebe, I. Cohen, A. Garg, and T. S. Huang, *Machine learning in computer vision*, vol. 29. Springer Science & Business Media, 2005.

[26] J. F. Allen, "Natural language processing," in *Encyclopedia of computer science*, pp. 1218–1222, 2003.

[27] M. Malheiros, C. Jennett, S. Patel, S. Brostoff, and M. A. Sasse, "Too close for comfort: A study of the effectiveness and acceptability of rich-media personalized advertising," in *Proceedings of the SIGCHI conference on human factors in computing systems*, pp. 579–588, 2012.

[28] J. MacQueen *et al.*, "Some methods for classification and analysis of multivariate observations," in *Proceedings of the fifth Berkeley symposium on mathematical statistics and probability*, vol. 1, pp. 281–297, Oakland, CA, USA, 1967.

[29] S. Chawla and A. Gionis, "k-means–: A unified approach to clustering and outlier detection," in *Proceedings of the 2013 SIAM International Conference on Data Mining*, pp. 189–197, SIAM, 2013.

[30] M. Mahajan, P. Nimbhorkar, and K. Varadarajan, "The planar k-means problem is np-hard," in *International Workshop on Algorithms and Computation*, pp. 274–285, Springer, 2009.

[31] M. K. Pakhira, "A linear time-complexity k-means algorithm using cluster shifting," in *2014 International Conference on Computational Intelligence and Communication Networks*, pp. 1047–1051, IEEE, 2014.

[32] F. Murtagh, "A survey of recent advances in hierarchical clustering algorithms," *The computer journal*, vol. 26, no. 4, pp. 354–359, 1983.

[33] F. Pedregosa, G. Varoquaux, A. Gramfort, V. Michel, B. Thirion, O. Grisel, M. Blondel, P. Prettenhofer, R. Weiss, V. Dubourg, J. Vanderplas, A. Passos,

D. Cournapeau, M. Brucher, M. Perrot, and E. Duchesnay, "Scikit-learn: Machine learning in Python," *Journal of Machine Learning Research*, vol. 12, pp. 2825–2830, 2011.

[34] C. Shalizi, "Distances between clustering, hierarchical clustering," *Lectures notes*, 2009.

[35] M. Dash and H. Liu, "Feature selection for classification," *Intelligent data analysis*, vol. 1, no. 3, pp. 131–156, 1997.

[36] O. Sharir, B. Peleg, and Y. Shoham, "The cost of training nlp models: A concise overview," *arXiv preprint arXiv:2004.08900*, 2020.

[37] M. Kukacka, "Overview of deep neural networks," *WDS '12 Proc. of Contributed Papers*, 2012.

[38] J. Zhang, C. Zong, *et al.*, "Deep neural networks in machine translation: An overview." *IEEE Intell. Syst.*, vol. 30, no. 5, pp. 16–25, 2015.

[39] J.-G. Lee, S. Jun, Y.-W. Cho, H. Lee, G. B. Kim, J. B. Seo, and N. Kim, "Deep learning in medical imaging: general overview," *Korean journal of radiology*, vol. 18, no. 4, p. 570, 2017.

[40] F. Qiu and J. Jensen, "Opening the black box of neural networks for remote sensing image classification," *International Journal of Remote Sensing*, vol. 25, no. 9, pp. 1749–1768, 2004.

[41] S.-C. Wang, "Artificial neural network," in *Interdisciplinary computing in java programming*, pp. 81–100, Springer, 2003.

[42] A. F. Agarap, "Deep learning using rectified linear units (relu)," *arXiv preprint arXiv:1803.08375*, 2018.

[43] L. Lu, Y. Shin, Y. Su, and G. E. Karniadakis, "Dying relu and initialization: Theory and numerical examples," *arXiv preprint arXiv:1903.06733*, 2019.

[44] D. Misra, "Mish: A self regularized non-monotonic neural activation function," *arXiv preprint arXiv:1908.08681*, vol. 4, 2019.

[45] N. Srivastava, "Improving neural networks with dropout," *University of Toronto*, vol. 182, no. 566, p. 7, 2013.

[46] S. Santurkar, D. Tsipras, A. Ilyas, and A. Madry, "How does batch normalization help optimization?," *arXiv preprint arXiv:1805.11604*, 2018.

[47] K. Krippendorff, "Mathematical theory of communication," *Departmental Papers (ASC)*, p. 169, 2009.

[48] C. E. Shannon, "A mathematical theory of communication," *ACM SIGMOBILE mobile computing and communications review*, vol. 5, no. 1, pp. 3–55, 2001.

[49] D. P. Kingma and J. Ba, "Adam: A method for stochastic optimization," *arXiv preprint arXiv:1412.6980*, 2014.

[50] D. Friedmann-Morvinski, "Glioblastoma heterogeneity and cancer cell plasticity," *Critical Reviews™ in Oncogenesis*, vol. 19, no. 5, 2014.

[51] Z.-M. Zhang, S. Chen, and Y.-Z. Liang, "Baseline correction using adaptive iteratively reweighted penalized least squares," *Analyst*, vol. 135, no. 5, pp. 1138–1146, 2010.

Appendices

Appendix A

Feature Selection

Features extracted from the original dataset: 509, 521, 522, 523, 524, 525, 526, 527, 528, 529, 530, 532, 533, 538, 539, 540, 541, 545, 546, 547, 548, 549, 550, 551, 552, 553, 562, 563, 647, 1449, 1450, 1451, 1452, 1453, 1454, 1455, 1456, 1457, 1458, 1459, 1460, 1461, 1462, 1463, 1464, 1465, 1468, 1469, 1470, 1471, 1472, 1473, 1474, 1475, 1476, 1477, 1478, 1479, 1480, 1481, 1482, 1483, 1484, 1485, 1487, 1492, 1494, 1495, 1496, 1497

Features extracted from the curated training set: 23, 30, 31, 297, 298, 299, 308, 309, 310, 508, 509, 521, 522, 523, 524, 525, 526, 528, 529, 647, 648, 722, 1494, 1496, 1501, 1681, 1685, 1686, 1692, 1696, 1697, 1699, 1700, 1701, 1702, 1703, 1704, 1705, 1706, 1707, 1708, 1709, 1710, 1711, 1712, 1713, 1714, 1715, 1716, 1717, 1718, 1719, 1720, 1721, 1722, 1723, 1724, 1725, 1726, 1727, 1728, 1729, 1730, 1731, 1732, 1733, 1734, 1735, 1736, 1737

Intersection among the feature sets: 509, 521, 522, 523, 524, 525, 526, 528, 529, 647, 1494, 1496

Appendix B

Spectral Images For Outlier Detection
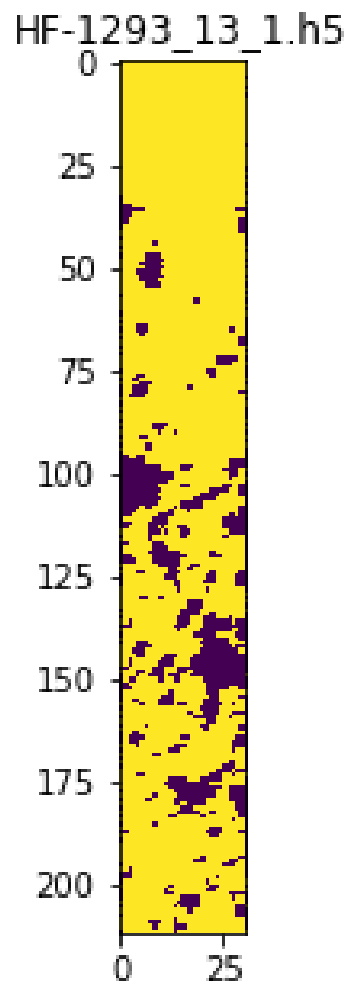
Figure B.1: The frequency criterion on sample HF-1293 from LGm1. The upper part of the sample also includes some outliers which the criterion fails to capture.
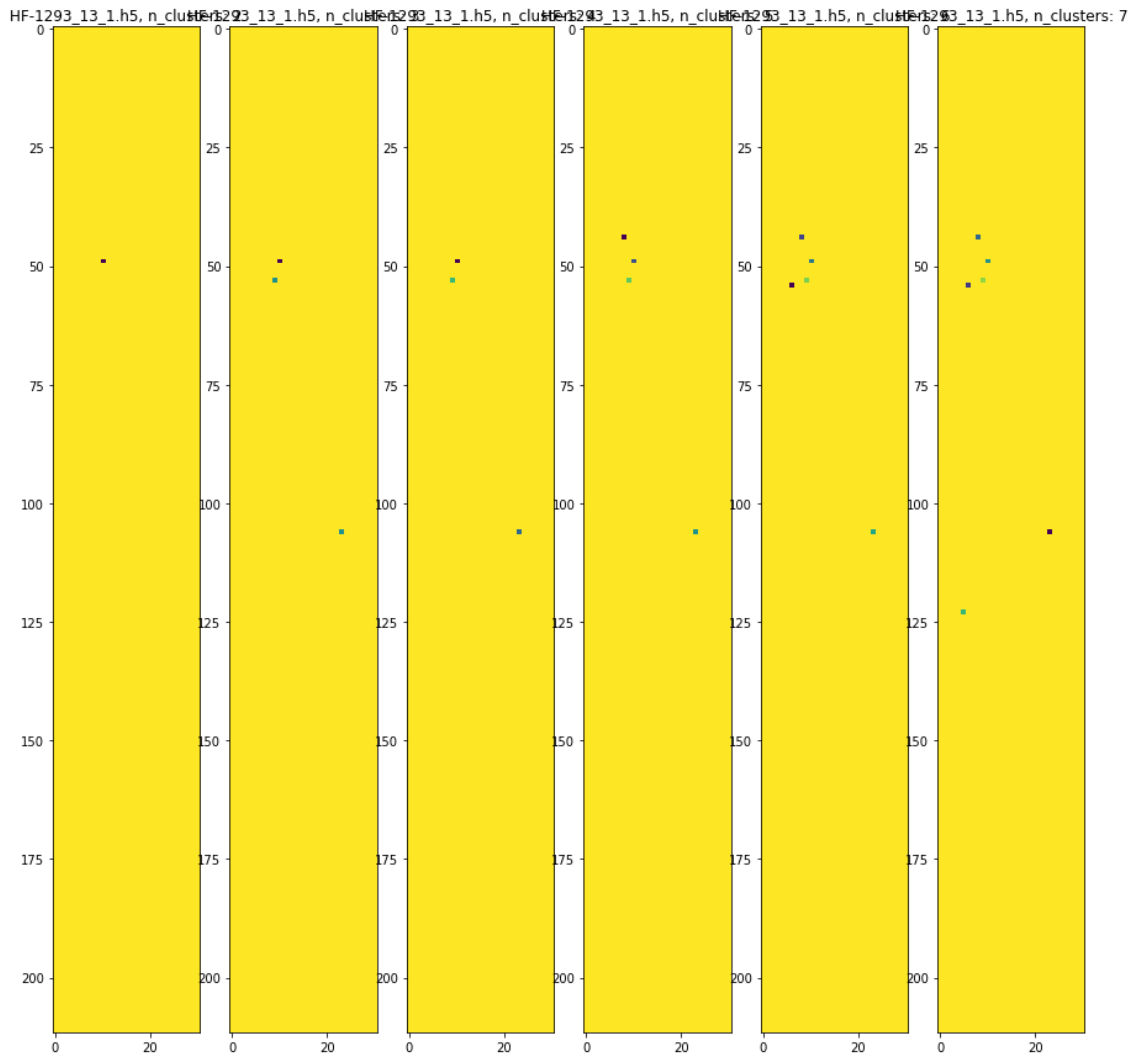
Figure B.2: Single linkage on sample HF-1293 from LGm1. Few regions are detected, the number of clusters required to detect all outliers are unknown.
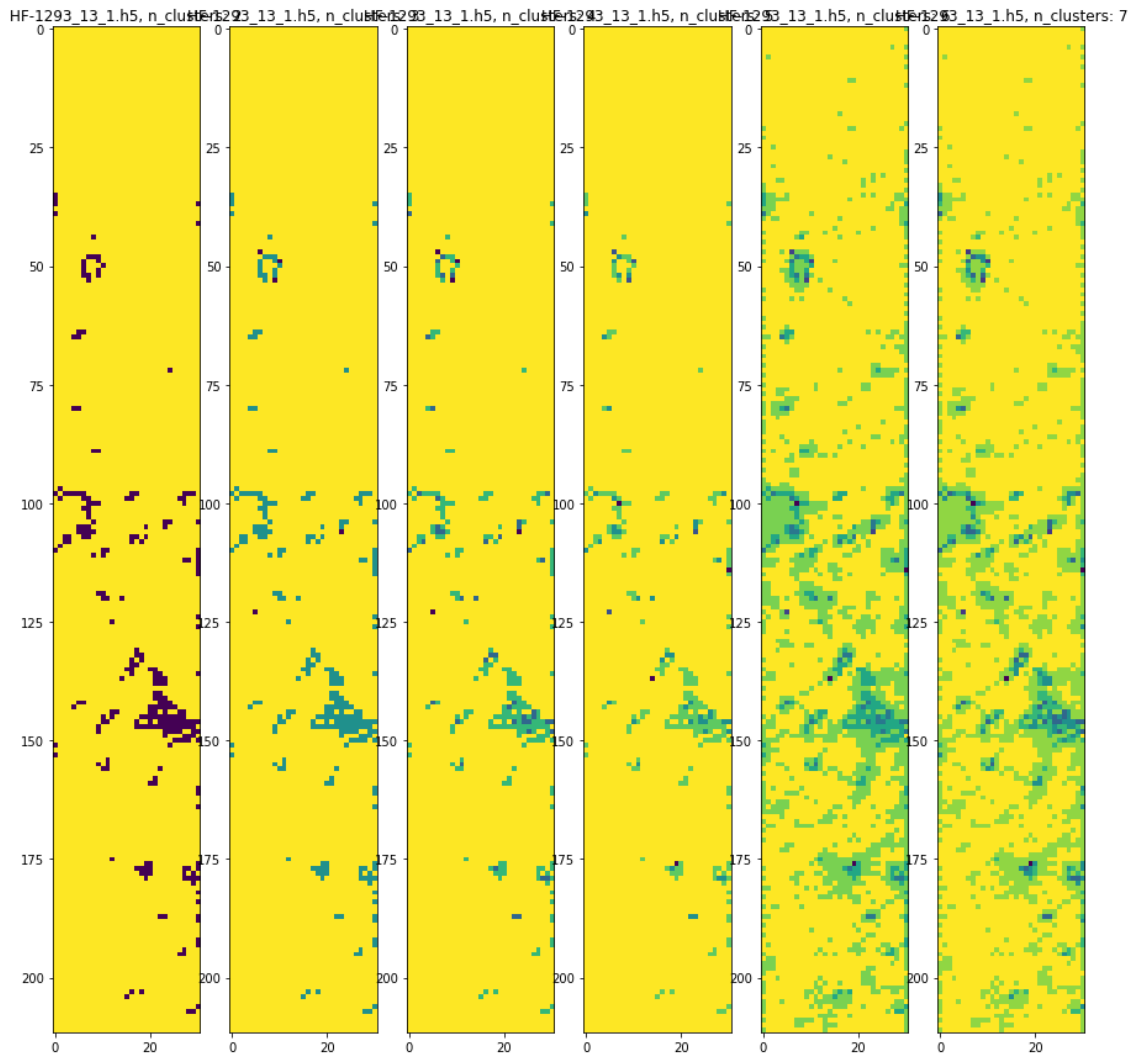
Figure B.3: Complete linkage on sample HF-1293 from LGm1. Some areas are detected with two clusters. Six clusters and up appear to capture most outliers.
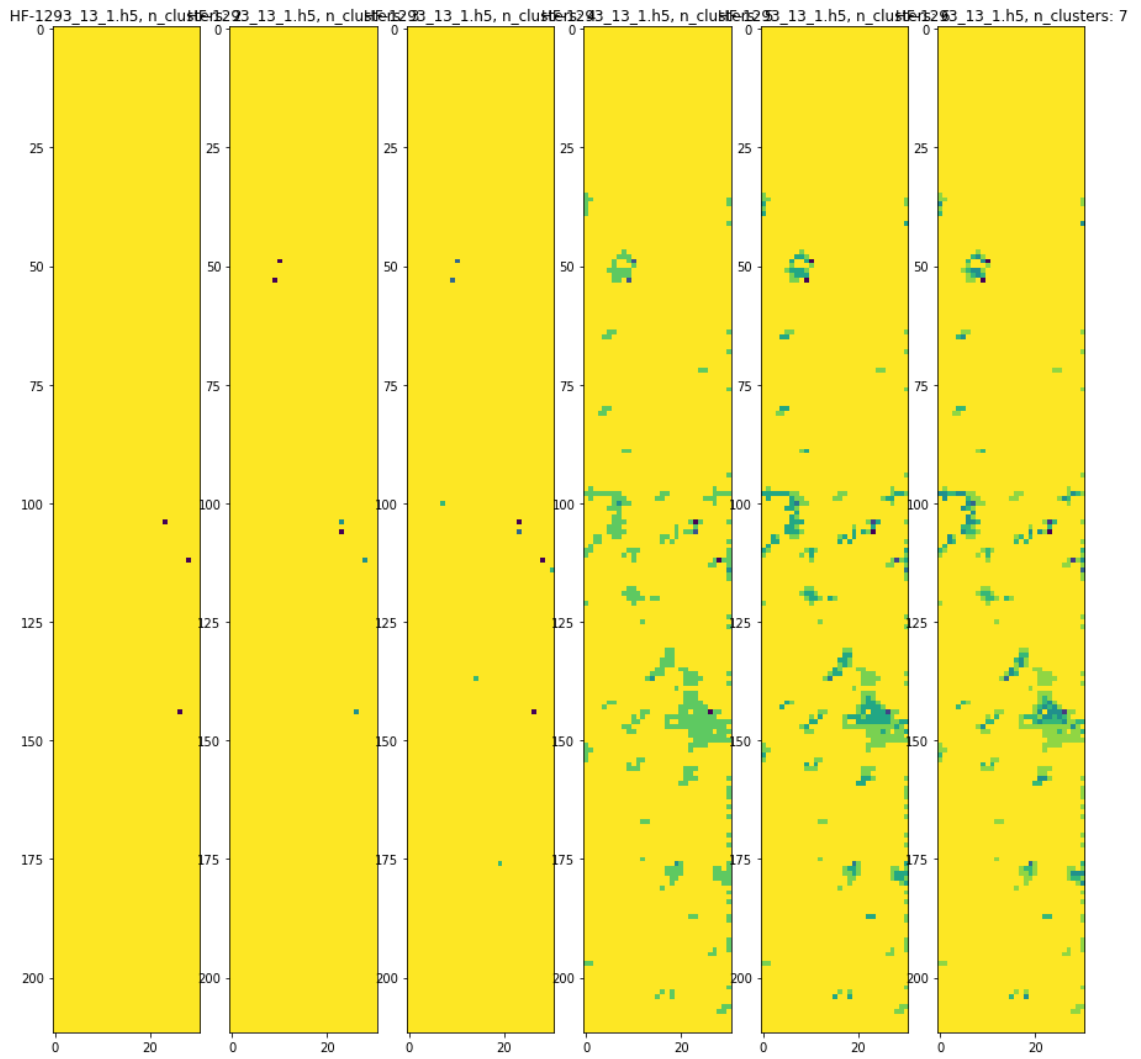
Figure B.4: Average linkage on sample HF-1293 from LGm1. With six clusters the same areas appear to be captured as those captured with two clusters when using complete linkage.
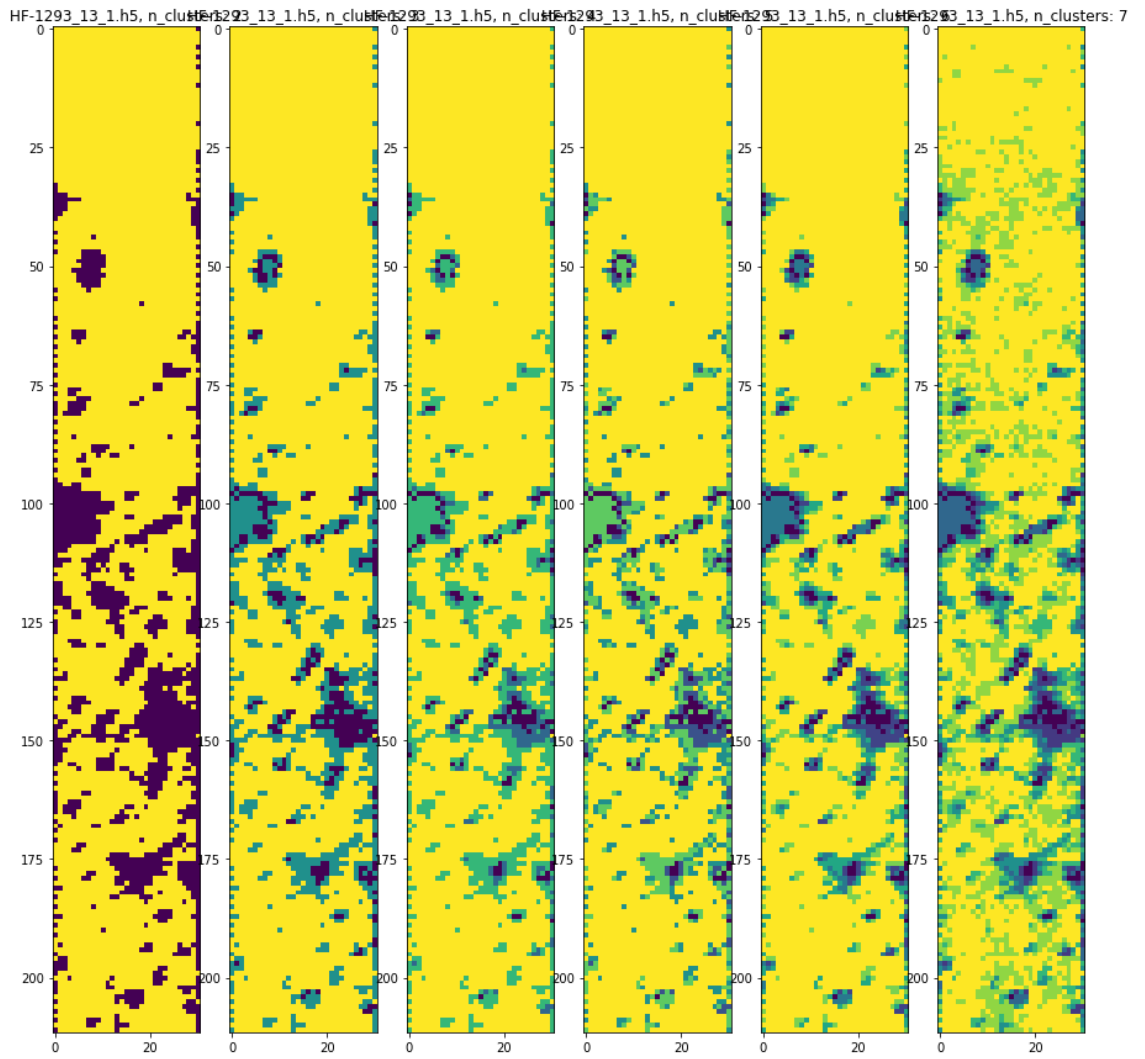
Figure B.5: Ward linkage on sample HF-1293 from LGm1. Overwhelming correspondence with the frequency criterion with only two clusters.
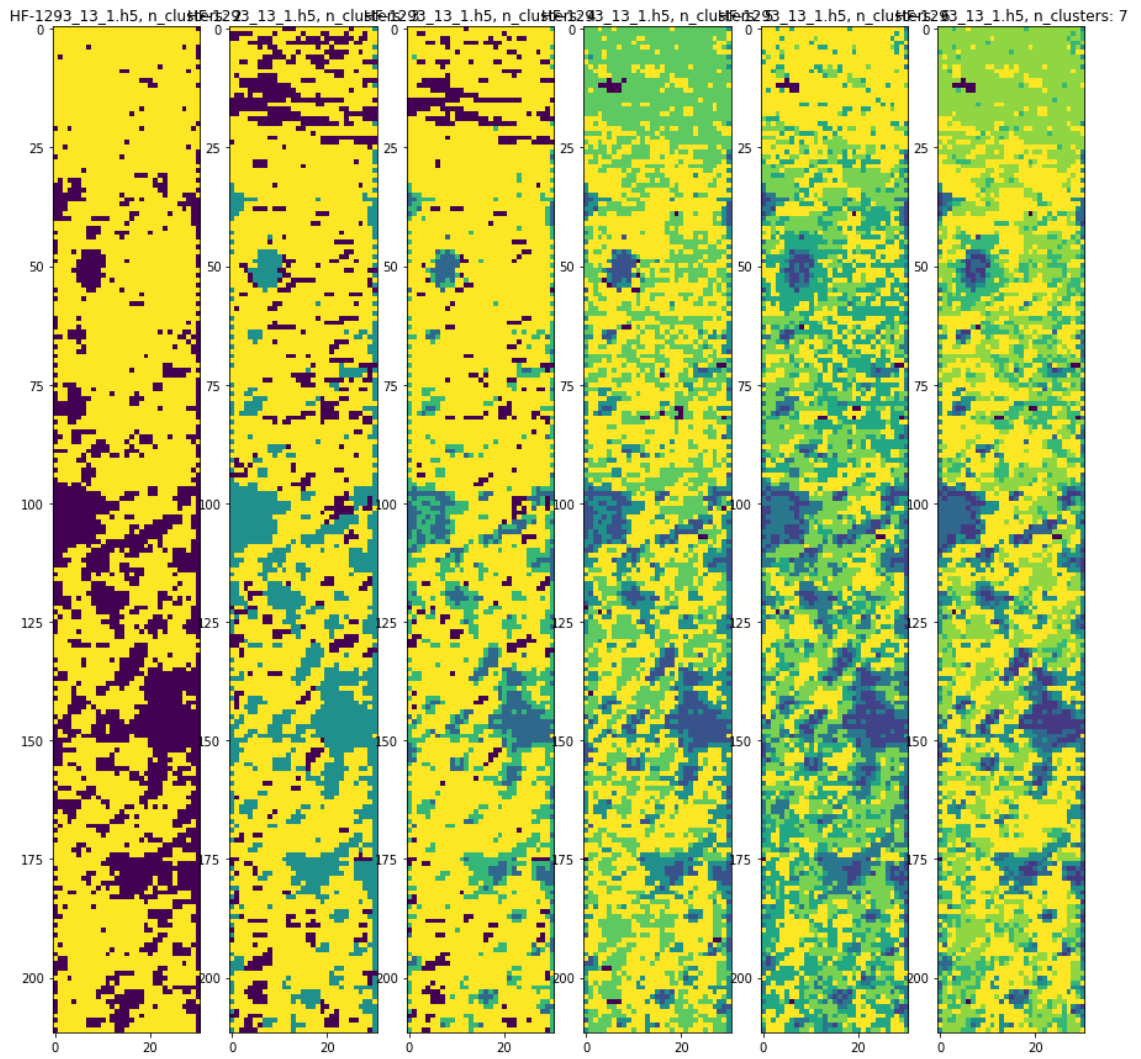
Figure B.6: K-means on sample HF-868 from LGm1. This is the only method capable of detecting the above region. All models computing more than two clusters detect outliers in the upper part.

Appendix C

Confusion matrix from model predictions

Figure C.1: The confusion matrix of the predictions for the separated training set. The diagonal shows the correct predictions of the models, wrong predictions are the surrounding area. The values within the cells are the number of predictions for the class. The model can generalize well to the separated training set.

Figure C.2: The confusion matrix of the predictions for the validation set. The validation set consists of samples not included in the training data. The samples are hard to generalize to. Only LGm1 is correctly labeled by the majority of predictions.
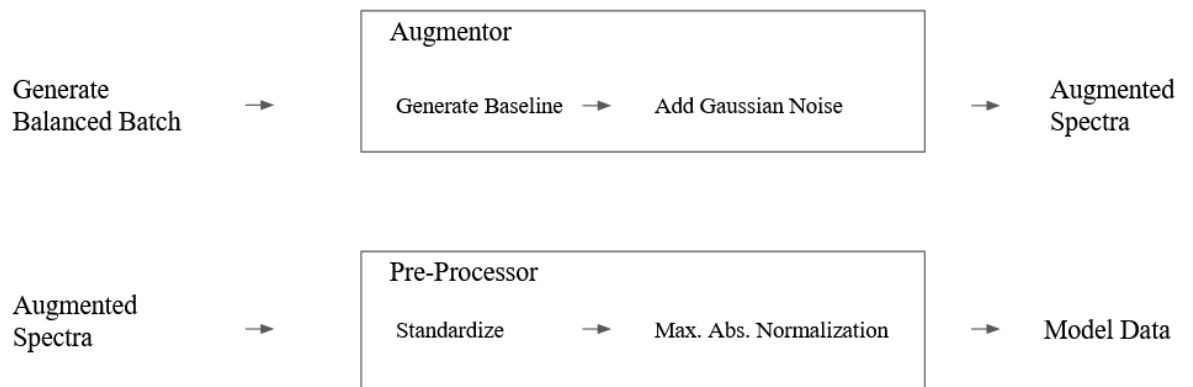
Appendix D

Pre-Processing Pipeline

Figure D.1: The pre-processing pipeline presented in Chapter 4. A batch of spectra with an equal number of spectra from each category is drawn from the training set. Each spectrum is then given a random baseline and additive Gaussian noise. The augmented data is then passed to the pre-processor which scales the data to a limited range.
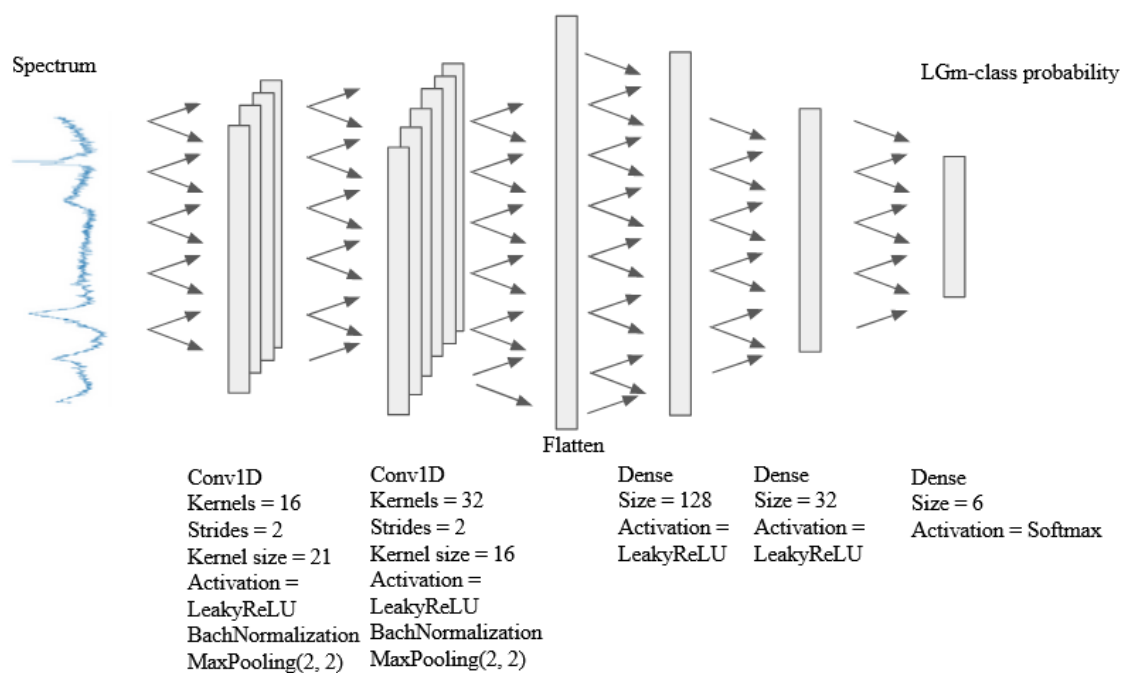
Appendix E

Model Architecture

Figure E.1: The model architecture trained in the project. The input spectrum must be pre-processed. The network has five layers, the middle box represents the flattened data following propagation through the two initial convolutional layers. The input is then propagated through the dense layers to the last layer where the input has been transformed to a probability distribution, i.e., the sum of the signals equals 1.